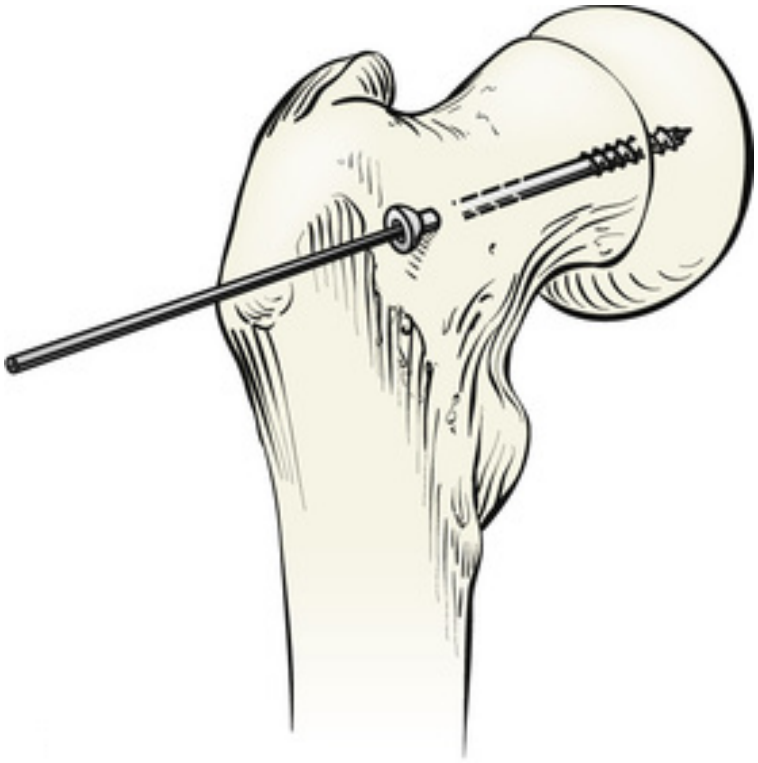
Evaluation of the screw position for in-situ fixation of slipped capital femoral epiphysis using finite element modelling



S.V. Cox

A thesis presented for the degree of
Master in Mechanical Engineering

Faculty of Mechanical Engineering
Department of BioMechanical Engineering
Biomaterials & Tissue Biomechanics
Delft University of Technology
October 8, 2024

TU Delft

Thesis committee:	Dr. Ir. N. Tümer	TU Delft	Supervisor
	Dr. Jaap Tolk	Erasmus MC	Supervisor
	Dr. Ir. B. Fereidoonnezhad	TU Delft	Committee member
	Dr. Ir. J. Zhou	TU Delft	Committee member
	M. Roelen	Erasmus MC	Committee member

This thesis is defended publicly on Friday the 18^{th} *of October* 2024*, at* 14:00*.*

Acknowledgements

I would like to thank my supervisor prof. Nazli Tumer for introducing me to this interesting research topic and connecting me to relevant clinicians at the Erasmus MC. I would also like to thank her for her guidance during this project, fruitful discussions, steering when needed and brainstorming about potential pipelines. I enjoyed our collaboration and thank her for that. Next, I would like to thank prof. Jaap Tolk for supervising me on the clinical perspective and offering knowledgeable insight. Furthermore, I would like to thank Merel Roelen and Eline van Es for helping me interpret the dataset and allowing me to use software at the Erasmus MC. To conclude I would like to thank my family and friends for always providing a listening ear and supporting me throughout the process.

Contents

1 Introduction **5**
- 1.1 Background . . . 5
- 1.2 Objectives . . . 6
- 1.3 Structural outline . . . 6

2 Methodology **6**
- 2.1 Healthy femur growth model . . . 7
  - 2.1.1 Software . . . 7
  - 2.1.2 Patient data . . . 7
  - 2.1.3 Segmentation of the femur . . . 7
  - 2.1.4 Growth plate generation . . . 8
  - 2.1.5 Mesh generation . . . 10
  - 2.1.6 Material Properties . . . 11
  - 2.1.7 Loading and boundary conditions . . . 12
  - 2.1.8 Analysis . . . 13
- 2.2 SCFE femur growth model . . . 15
  - 2.2.1 Patient data . . . 15
  - 2.2.2 FE model . . . 15
  - 2.2.3 SCFE screws . . . 16
  - 2.2.4 Locations of the screws . . . 17
  - 2.2.5 SCFE loading and boundary conditions . . . 17
  - 2.2.6 Analysis . . . 19

3 Results **23**
- 3.1 Healthy femoral growth . . . 23
  - 3.1.1 Stresses in the femur . . . 23
  - 3.1.2 Stresses in the growth plate . . . 25
  - 3.1.3 Comparison to Roels et al. [1] . . . 27
  - 3.1.4 Comparison to CT scan data . . . 29
- 3.2 SCFE femoral growth . . . 31
  - 3.2.1 Instant mechanical growth (external load only) . . . 31
  - 3.2.2 Sensitivity study . . . 34
  - 3.2.3 Long-term growth . . . 39

4 Discussion **47**
- 4.1 Healthy growth analysis . . . 47
- 4.2 ABAQUS vs MIMICS growth plate generation . . . 47
- 4.3 SCFE Instant growth . . . 48
- 4.4 SCFE long-term growth . . . 48
- 4.5 Comparison to Slobbe et al. [2] . . . 49
- 4.6 FE model generation . . . 49
- 4.7 Growth Analysis . . . 51
- 4.8 Recommendations for future work . . . 52
- 4.9 Conclusion . . . 53

A Patient data - SCFE femur **59**

B Segmentation parameters healthy femur - ABAQUS method **60**

C Segmentation parameters healthy femur - MIMICS method **61**

D Segmentation parameters SCFE femur **62**

E Segmented growth plate material elements **63**

F Bone-implant interaction in literature **64**

G Biological growth rate computation **66**

H ABAQUS versus Python visualisation **67**

I Python scripts **68**

Abstract

Slipped Capital Femoral Epiphysis (SCFE) is the most common hip disorder in adolescents characterised by the displacement of the femoral head relative to the femoral neck through the growth plate [3]. In-situ fixation, the current standard type of treatment, stabilises the epiphysis to prevent further slippage. Although it prevents further slippage of the femoral head, the altered morphology of the proximal femur remains [4], leading to long-term complications. Recent studies have, however, revealed that bone growth can continue after fixation, suggesting potential for guided bone growth through strategic screw placement. The aim of this study is to find the optimal screw position for in-situ fixation to stimulate longitudinal bone growth in desired areas, thereby potentially improving the femur morphology and reducing SCFE severity. The study is divided into two parts: the first part focuses on modeling healthy bone growth to validate the computational approach against results from a prior study and clinical data, while the second part concentrates on SCFE analysis to explore the optimal screw position for in-situ fixation to stimulate longitudinal bone growth in desired areas. A finite element (FE) model of a femur with a mild slip was developed to predict bone growth under various screw positions. The Osteogenic Index (OI), which quantifies the expected amount of bone growth, was used to predict growth patterns. The findings indicate that the conventional center-center screw position, commonly used in surgical practice, results in minimal bone growth. Conversely, anteriorly positioned screws, particularly in the anteromedial (AM) and anterolateral (AL) regions, were associated with the most significant and beneficial growth on the posterior side of the growth plate. The expected amount of growth in the AM and AL positions was approximately 211% and 138% greater, respectively, than in the conventional center-center position. These results suggest that anterior screw placement could enhance bone growth in desired areas, potentially mitigating the severity of SCFE and improving long-term functional outcomes. These results reinforce similar findings of a prior retrospective clinical study by [2]. This study contributes to a growing body of evidence supporting the reconsideration of traditional screw placement strategies in SCFE treatment. The insights gained could inform surgical practices aimed at optimising growth modulation and improving patient outcomes. Recommendations have been given to improve the FE analysis and validation. The largest uncertainty lies in the hip contact force in SCFE patients. Further research is needed to investigate this loading for different patients and slip severities and test the influence of the loading conditions on the growth pattern. In addition, clinical trials are necessary to fully validate these findings and assess their practical implications in the treatment of SCFE.

1 Introduction

1.1 Background

Slipped Capital Femoral Epiphysis (SCFE) is a prevalent orthopedic condition in adolescents, characterised by the displacement of the epiphysis relative to the metaphysis through the growth plate (physis) in posterior and inferior direction [5]. It is more prevalent in boys than in girls and has a direct correlation with body weight, with the average onset of SCFE around 12 years of age [3, 6]. The condition can lead to significant complications, including loss of motion, pain, early onset of osteoarthritis [3, 6, 7] as well as osteonecrosis and chondrolysis [5].
The standard form of treatment for SCFE is in-situ fixation, which stabilises the epiphysis and prevents further slippage. Current guidelines suggest to place the screw in the center of the femoral head and to have a minimum of four threads across the physis [5]. The screw should not be closer than $2.5-5$ mm to the joint surface [8]. Slip progression after in-situ fixation only potentially occurs in cases with less than four screw threads in the epiphysis, with the slip progression inversely related to the number of screw threads in the epiphysis [9, 10]. This method has shown to be favourable over other types of treatment in terms of long-term outcomes and delay of degenerative arthritis [11]. Although in-situ fixation prevents progressive deformity of the proximal femur, the altered proximal femur morphology persists [4]. The abnormal femoroacetabular geometry and mechanics can result in hip pain associated with loss of flexion and internal rotation and antalgic gait [4] and comes with risks of femoroacetabular impingement (FAI) and early hip osteoarthritis [12, 13]. In severe cases this might necessitate total hip arthroplasty later in life. It is for this reason that some suggest to use capital realignment procedures instead [14], but this procedure comes with the risk of significant postoperative complications such as femoral head avascular necrosis, fixation failure with deformity progression, or postoperative hip dislocation [15]. Historically, it was believed that in-situ fixation would lead to physeal arrest due to the stabilisation of the growth plate [16]. The primary goal of screw fixation was merely to prevent further slippage. However, recent findings have challenged this notion, showing that bone continues to grow even after in-situ fixation [2]. This persistent growth has prompted the development of dynamic screws capable of extending to accommodate this remaining bone growth [17]. More importantly, the finding that there still exists growth potential after screw placement in SCFE patients is crucial for this research, as it opens the possibility of guided bone growth in desired directions. This guided growth could potentially lead to a more natural femoroacetabular geometry and reduce complications associated with SCFE. The hypothesis, reinforced by the findings of a study by [2], is that by strategically placing the screw, it may be feasible to encourage the femoral head to move closer to its original anatomical position, thereby reducing the severity of the slip. Considering that the usual femoral shaft displacement in SCFE patients is anteromedial, growth on the posterior side of the growth plate is desirable to counteract this deformity. The influence of the screw position on stresses within the growth plate and subsequent bone growth is a critical consideration in optimising SCFE treatment. The positioning of the screw can alter the mechanical environment of the growth plate, potentially influencing the direction and magnitude of bone growth. Understanding both the biological and mechanical factors influencing bone growth and the interplay between the two is crucial for improving SCFE management. Computational growth modeling has emerged as a powerful tool to simulate and predict bone growth under various mechanical loads. Despite the advances in bone remodeling and bone-implant interaction modeling, there is a notable gap in the research regarding the computational modeling of bone growth originating from the physis, particularly in the context of SCFE. Recent studies, including the retrospective clinical study by

[2], have highlighted the importance of screw positioning in growth outcomes. They found that a significant but limited amount of growth can be expected after in-situ screw fixation, with the amount of growth influenced by the severity of the slip and the position of the screw. The outcomes suggest that targeted screw placement could strategically induce shear stresses and tensile stresses in the right areas, positively influencing bone growth in desired regions.

1.2 Objectives

The aim of this study is to find the optimal screw position for in-situ fixation of SCFE to stimulate bone growth in a manner that mitigates the severity of the slip. To do so, a computational bone growth model is set up including both biological and mechanical factors. By evaluating the areas of expected bone growth and comparing these to the desired areas of growth, this study can be used to aid in medical intervention decisions and more specifically to find the optimal screw position for surgical interventions in patients suffering from SCFE.

Research Questions

The primary research question is: What is the optimal screw position for in-situ fixation of slipped capital femoral epiphysis to stimulate longitudinal bone growth on the posterior side of the growth plate?

1.3 Structural outline

This first chapter formed the introduction into the topic and research. In Chapter 2 the methodology of the study is presented. This study consists of two parts: 1) the modelling of healthy femoral growth and 2) the modelling of growth in a SCFE femur fixed with a screw in different potential positions. The first part was performed to understand healthy bone growth and to validate the model by comparing results to those of another computational bone growth study. In the second part, bone growth in a SCFE femur fixed with a screw was investigated to answer the research question. The next chapter explains how the FE models of both the healthy femur and the SCFE femur are created and how the analysis is performed. Chapter 3 presents the results of the analyses and in Chapter 4 the results are discussed and a conclusion is given.

2 Methodology

As mentioned before, this study consists of two different parts: the modelling of healthy bone growth and the modelling of a femur with slipped capital femoral epiphysis. The necessity of the first part is twofold: 1) comparing the healthy growth results to another study and thereby validating the scheme followed to generate the FE model and 2) evaluating the effects of two different growth plate generation strategies on the stress patterns in the femur and growth plate, which will influence the SCFE methodology. The generation of healthy and SCFE femur FE models consists of several steps as can be seen in Figure 1, which are presented in this chapter.

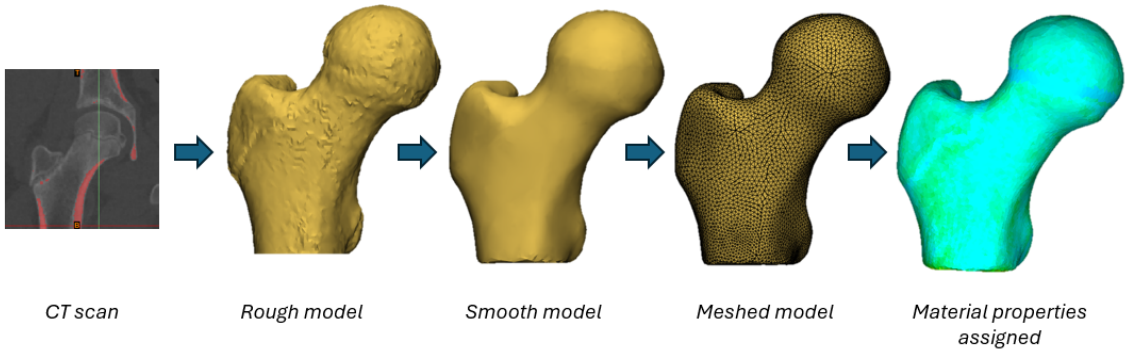


Figure 1: The process of creating the femur model. The different steps are described in the subsections of this chapter.

2.1 Healthy femur growth model

The 3D model of the femur was created using Mimics and 3-Matic (Materialise, Belgium). The first was used for segmentation of the bone from CT scan data, creation of the growth plate and for material assignment. The latter was used to discretise the 3D reconstructed femur based on the segmentation results. The full process of creating a finite element model is visualised in Figure 1.

2.1.1 Software

This study made use of Mimics 26.0 and 3-matic 18.0 (Materialise, Belgium) for segmentation, growth plate generation, meshing and material assignment, ABAQUS (Dassault Systèmes Simulia Corp) for finite element analysis and Python 3.10.7 for post-processing. The following external packages were used: NumPy 1.26.4 for numerical computations and mathematical functions and Matplotlib 3.9.0 for the visualisation of results (the Poly3DCollection class of the mpl_toolkits.mplot3d.art3d package was used for creating three-dimensional polygon collections).

2.1.2 Patient data

For the creation of the 3D model, a dataset available at the Erasmus MC, which consists of computed tomography (CT) scans of patients treated for SCFE, was used. The unaffected femur of a patient on a bilateral CT scan was used for the healthy growth modelling. This bilateral scan was made using a Siemens SOMATOM Definition Flash scanner with the following acquisition parameters: x-ray exposure 120kV and 96mAs, display field of view 75.6 x 38.3 cm and slice thickness 1.0 mm. The patient is an 11 year old girl with a height of 163 cm and a body weight of 77 kg. The follow-up CT scan was taken 30 months later. This bilateral CT scan was made using a Siemens SOMATOM Drive scanner with x-ray exposure 110kV and 267mAs, display field of view 32.0 x 32.7 cm and slice thickness 2.0 mm.

2.1.3 Segmentation of the femur

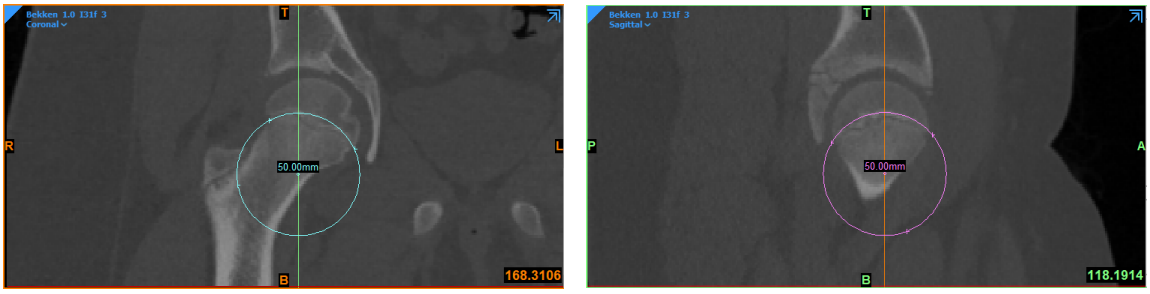
The femur was segmented from the CT scan images in the image processing software Mimics using region grow, split mask and smart fill. This was done to create the femur as a part, which was

then used in 3-Matic. The parameters for the segmentation of the femur using both growth plate generation techniques explained in the next section are shown in Appendices B and C.

2.1.4 Growth plate generation

Two different methods were employed to create the growth plate. In the first method (hereafter named *the ABAQUS method*) the growth plate was created in ABAQUS after generating the mesh and in the second method (named *the MIMICS method*) the growth plate was generated in Mimics before generating the mesh. The first method is much easier and hence faster to implement. The hypothesis, however, is that the second method leads to more accurate results because the growth plate is taken into account when generating the mesh, leading to a smoother growth plate region surface. Therefore, both methods were tested to investigate the differences between the results of both methods. Both methods are explained in the subsections below.

In both methods, the growth plate was generated by fitting a sphere to the femur at the growth plate site to create a convex growth plate, like done in the study by [1]. To determine the optimal sphere diameter and position, the sphere was manually adjusted by scrolling through the CT scan slices in both the coronal and sagittal views. The sphere was positioned in the center of the thickness of the growth plate at both edges. Figure 2 shows that the fitted sphere does not perfectly match the actual shape of the growth plate, indicating that the growth plate is not a perfect sphere in reality. However, for simplicity and to be able to compare the outcomes of this study to those of other studies, it was chosen to fit a sphere. The optimal diameter for the sphere was found to be 50 mm. The coordinates of the sphere's center and its diameter were later used to create the growth plate. A thickness of 3 mm was chosen for the growth plate, in line with the study by [1].



(a) (b)

Figure 2: The chosen diameter for the growth plate in the a) coronal and b) sagittal view.

Growth plate generation in ABAQUS

In the ABAQUS method, the femur was segmented in Mimics and the mesh was generated in 3-Matic, after which the model was exported to ABAQUS. In ABAQUS, the growth plate section was generated by finding the elements of the mesh that fell within the growth plate region. This was done using the function *getByBoundingSphere* in a Python script. The growth plate region was created using boolean operations on the element sets of two spheres (with the inner and outer

diameter of the growth plate) and the femur. This growth plate region was saved as a separate set, after which the material properties of the growth plate were assigned.

Growth plate generation in Mimics

To generate the growth plate in Mimics, masks of the inner and outer fitted sphere (which are shown in Figure 3) were created. The region of the growth plate was created using boolean operations on these masks, the mask of the femur and a mask of a cylinder (Figure 5), to let the growth plate fall completely within the femur. The masks of the growth plate and the rest of the femur were converted to parts and then exported to 3-Matic for meshing. The results of these part generations can be seen in Figure 4. The meshed parts were exported back to Mimics for material assignment using the previously created masks. The growth plate elements on the outside (close to the surface of the femur) that were not captured with this growth plate mask were later added to the growth plate region in ABAQUS using the function *getByBoundingsphere* in a Python script using the same method as described in the previous section. In addition, some elements that were part of the smooth growth plate but didn't receive the growth plate material properties through the material assignment method in Mimics, were manually added to the growth plate region in ABAQUS, thereby assigning growth plate material properties to these elements. This is visualised in Appendix E. In the Discussion this reasoning is further elaborated upon.

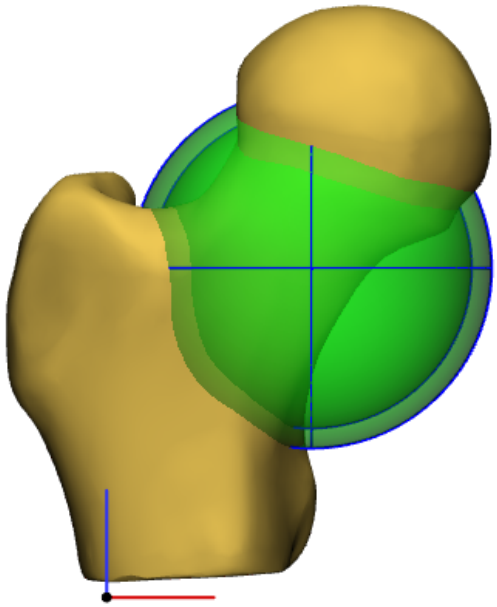


Figure 3: The fitted spheres used to create the growth plate.



Figure 4: The femur (in yellow) with the growth plate (in grey).

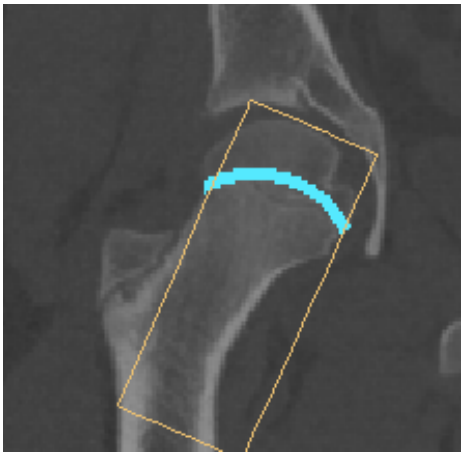


Figure 5: The cylinder used in the boolean operations of the masks to create a growth plate that falls completely within the femur.

2.1.5 Mesh generation

After the segmentation, the parts were exported to 3-Matic to create the mesh. Before generating the mesh, spikes were removed and the model was smoothed. To improve the initial mesh, the number of triangles was reduced with the function Quality Preserving Reduce Triangles. Hereafter the part was remeshed (surface mesh) with a target triangle edge length of 1.5 mm. The improvement after every performed operation in the surface remeshing can be seen in Table 1 in the form of the number of triangles. For the volume mesh, Tet4 elements were chosen (4-node linear tetrahedral elements (C3D4)) with a maximum edge length of 1.5 mm. Both the surface mesh and volume mesh edge lengths are chosen to be in accordance with those in the study by [1]. All parameters used for the generation of the mesh with the ABAQUS method and the MIMICS method can be found in Appendices B and C, respectively. A previous study by [1] included a convergence study for the optimal number and type of elements (considering computational time and accuracy of the results). 10-node quadratic tetrahedral elements (C3D10) were compared with 4-node linear elements (C3D4). Quadratic elements showed a slightly better performance, because they are better at curved surfaces, but the finest linear element mesh was chosen after considering the computational time. Therefore, these elements were also chosen in this study. For the method where the growth plate was generated in Mimics, the femur and growth plate parts were merged right before generating the volume mesh.

Operation	**Estimated number of triangles**
Initial	Femur: 35210, GP 7572
Quality preserving reduce triangles	Femur: 15416, GP: 3174
Uniform remesh	Femur: 15640, GP: 3361

Table 1: The number of triangles in the femur and growth plate (GP) after every performed operation during the surface remeshing.

As explained in the previous section, in one method the growth plate was generated *before* the generation of the mesh, and in another method the growth plate was generated *after* the generation of the mesh. This leads to two different meshes. The mesh of the ABAQUS method can be seen in Figure 6. Here a volume mesh of the entire femur was generated and the growth plate had not yet been created. The elements that were assigned the growth plate material properties in ABAQUS later on are visualised in yellow. Figure 7 shows the mesh of the MIMICS method. In this method the growth plate was created before the mesh, such that separate volume meshes were created for the growth plate and for the rest of the femur. These meshes were merged in 3-Matic before exporting back to MIMICS.

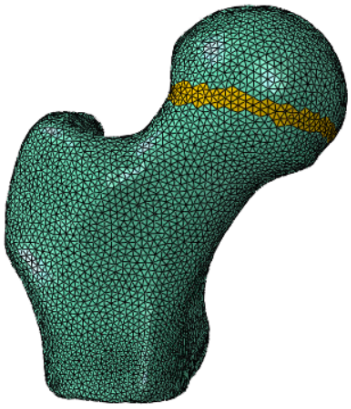


Figure 6: The ABAQUS method mesh (growth plate visualised in yellow).



Figure 7: The MIMICS method mesh. A separate volume mesh is created for the growth plate and the rest of the femur.

2.1.6 Material Properties

After creation of the mesh, the model was exported back to Mimics to assign the material properties. CT scans contain information about the radiodensity of different parts in the CT scan images in the form of Hounsfield units (HU) or greyscale units. These HU values can be related to density values. If there is no calibration phantom included with the CT scans, known density values can be used to find the relationship between the Hounsfield units and the density values. This assumes a linear relation between the two according to:

$$\rho = \alpha + \beta \cdot HU \tag{1}$$

By measuring the HU values of air and cortical bone on the CT scan and using the known density value for both, the α and β values can be found. The average HU values for air and for cortical bone on the CT scans were found to be -1024 and 947, as can be seen in Figure 8. Little is known about the mechanical properties of child bone tissue, due to the difficulty to collect such tissue, but one study investigating the mechanical properties of cortical bone found that the average bone mineral density in femurs and tibia of 12 children aged 4-15 was 0.9 g/cm^3 [18]. The density value for air is usually taken as $1.225 \cdot 10^{-3}$ g/cm^3. Using the measured HU values and these known density values for air and cortical bone, α and β were found to be 0.468 and 0.000456. Using these

values the density could be calculated for all regions of the bone using formula 1. A range of 200 bone density values was assigned to the femur using this equation in Mimics.

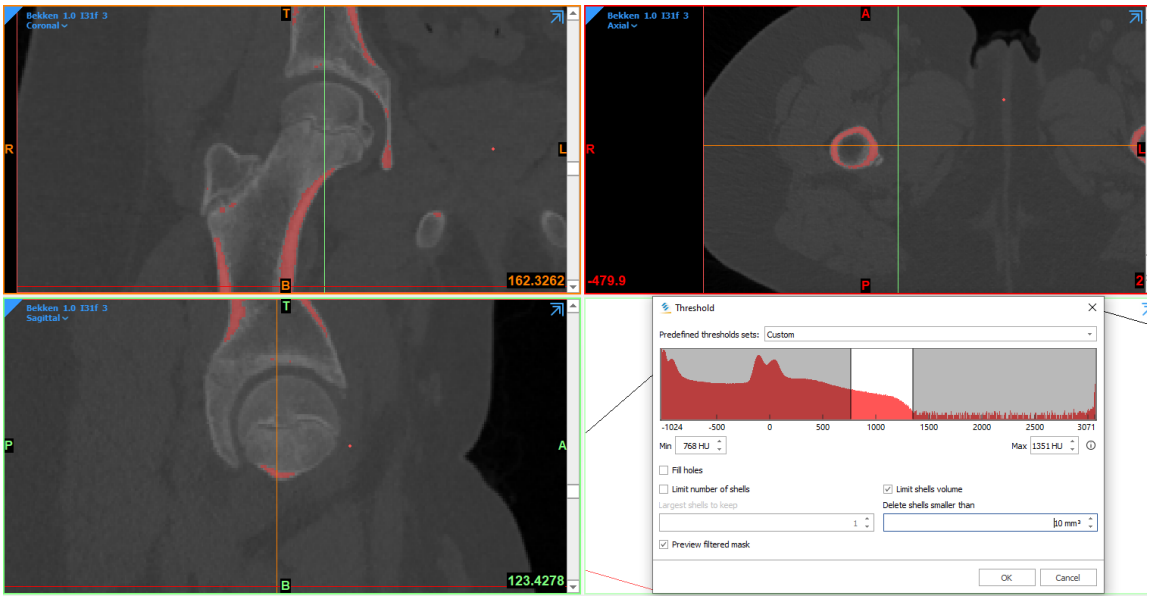


Figure 8: The cortical bone mask threshold region (red) used in Mimics. The range was 768 HU until 1351 HU. The average HU value for cortical bone was 947 HU.

The study by [18] furthermore found a relationship between bone mineral density and the elastic modulus of cortical bone tissue in children according to:

$$E = 12900 \cdot \rho^{2.0} \tag{2}$$

where E is the elastic modulus in MPa and ρ is the bone mineral density in g/cm^3 [18]. This equation was used to specify the elastic modulus in the bone. It was used in MIMICS to assign elastic modulus values to the mesh elements in the femur model. The average HU unit value for trabecular bone was 347, leading to an average elastic modulus of 5.1 GPa. The average HU unit value for cortical bone was 947, leading to an average elastic modulus of 10.4 GPa. This value is acceptable compared to the elastic modulus of 9.1 GPa found by [19] for cortical bone in children (4-16 years) through a three-point microbending test. This study furthermore mentioned that their result might be an underestimation of the elastic modulus due to the small span to depth ratio of the used bone samples. The mesh elements of both types of bone were modelled with a Poisson's ratio of 0.3. The growth plate was given a constant elastic modulus of 6 MPa and a Poisson's ratio of 0.49 as done in many other studies [1, 20, 21]. The FE model with the assigned material properties was then exported to ABAQUS.

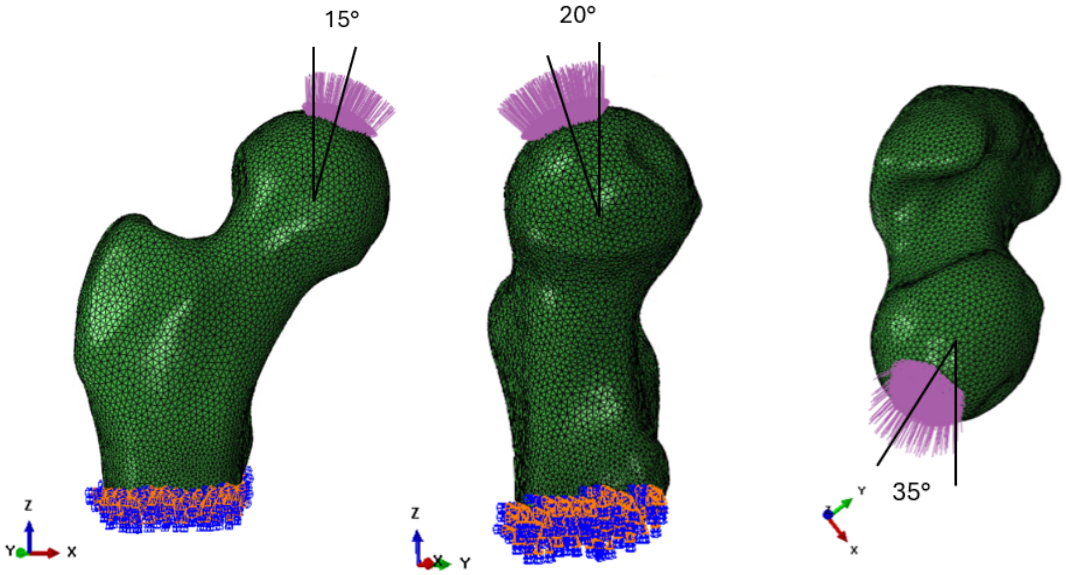
2.1.7 Loading and boundary conditions

Next, the loading conditions were assigned in ABAQUS. For the hip contact force the loading conditions from [22] and [23] as used by [1] were used. The study by [1] applied a concentrated

force on the center of the femoral head, representing the resultant hip contact force during normal gait. The body weight was used to compute the load magnitude according to:

$$F = m \cdot 10 \cdot 2.5 \tag{3}$$

such that 250% of the body weight was applied. The load was applied with an inclination angle of 15° in the coronal plane, 20° in the sagittal plane and 35° in the axial plane, as can be seen in Figure 9. The resultant hip contact force was applied as a pressure distributed over a circular area with a diameter of 15 mm. Hence, for the healthy growth patient a total force of 1925 N was applied. It was applied in a single step with a time period of 1. Only the hip contact force was applied, as this force contributes most to the stress distribution in the growth plate [24]. The distal end of the femur was fully constrained, such that no translations or rotations were possible.



(a) (b) (c)

Figure 9: The applied load on the femur. It is applied as pressure distributed over a circular area, with a total force of 1925 N. The load is applied with an inclination angle of 15° in the coronal plane, 20° in the sagittal plane and 35° in the axial plane, relative to the femoral head center.

2.1.8 Analysis

Longitudinal bone growth originates from the growth plate (physis) where cartilage is formed and subsequently calcified and degraded and replaced by osseous tissue; a process called endochondral ossification [25]. This process takes place until skeletal maturation, when the growth plate closes and longitudinal bone growth ceases. A variety of biological factors such as genetic, nutritional and hormonal factors, and mechanical factors affect longitudinal bone growth, as visualised in Figure 10. For the healthy growth study, the focus is on the effect of mechanical factors on bone growth (IIa in Figure 10) and the biological factors were not included, in accordance with the study by [1] to which the results of this analysis are compared.

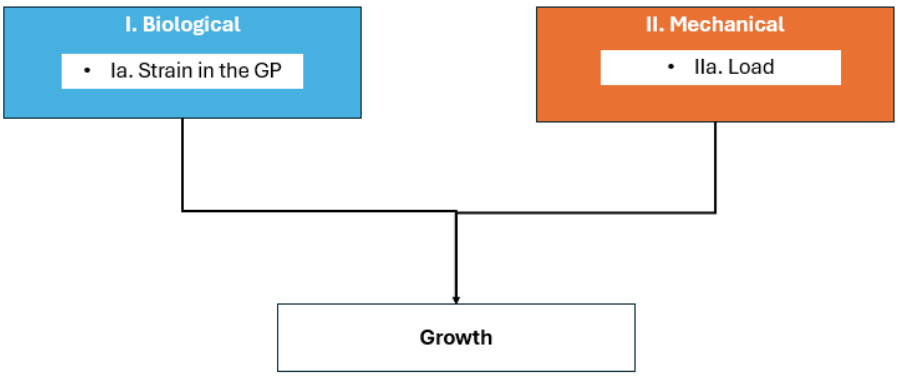


Figure 10: Factors influencing growth in the growth plate instantly after placement of the screw.

Calculation of Osteogenic Index

Mechanical loading is known to modulate endochondral ossification. Research by Carter et al. demonstrated that growth is accelerated by hydrostatic tensile stresses and octahedral shear stresses, and inhibited by hydrostatic compressive stresses [26]. A commonly used method for determining the mechanical component of bone growth is the use of the osteogenic index (OI) proposed by Carter:

$$OI = \dot{\epsilon}_m = a \cdot \tau_{oct} + b \cdot \sigma_h \tag{4}$$

where τ_{oct} is the octahedral shear stress (always positive), σ_h is the hydrostatic stress (negative in compression and positive in tension) and a and b are constants [27]. In the healthy growth study $a = 1$ and $b = 0.5$, leading to a ratio $b/a = 0.5$ in accordance with previous studies [28, 29, 30, 31, 32, 33]. The octahedral shear stress is calculated from the principal stresses according to:

$$\tau_{oct} = \frac{1}{3}\sqrt{(\sigma_1 - \sigma_2)^2 + (\sigma_2 - \sigma_3)^2 + (\sigma_3 - \sigma_1)^2} \tag{5}$$

and the hydrostatic stress, or octahedral normal stress, is calculated according to:

$$\sigma_h = \frac{\sigma_1 + \sigma_2 + \sigma_3}{3} \tag{6}$$

where $\sigma_1, \sigma_2, \sigma_3$ are the principal stresses [21, 34]. The OI is used in the FE analysis to compute and visualise the expected growth rate in different areas of the femur and growth plate.

FE model validation

The results of the healthy growth study are used to choose the growth plate generation method for the SCFE study. Furthermore the results are compared to results of a similar study by Roels et al. [1] to validate the methodology. The study by Roels et al. investigated the influence of different loading conditions and growth plate shapes on cam-type deformities. The study found that specific loading patterns modify the distribution of the mechanical stimulus and thereby stimulate the development of cam-type deformity. A loading scenario of the study by Roels et al. representing the resultant hip contact force in a normal walking cycle was reproduced (see section 2.1.7). The

stress patterns in the femur and growth plate for this loading condition are compared to the results of the study by Roels et al. in the case of using a convex growth plate generated with the ABAQUS method, to validate the methodology for generating the FE model. In addition to the comparison with the results of the study by Roels et al, the results are also compared to the change in neck-shaft angle (NSA) measured on the baseline and follow-up CT scans of the healthy growth patient.

2.2 SCFE femur growth model

The method of creating a FE model for the SCFE femur is similar to the method for the healthy femur as explained in section 2.1. However, some steps are slightly different and some additional steps are needed. These are explained in this chapter.

2.2.1 Patient data

For the SCFE study, a patient with a moderate slip was chosen from the dataset of the Erasmus MC. The patient is an 11 year old girl with a height of 163 cm and a body weight of 77 kg. Additional SCFE-related measurements taken of the femur can be found in Appendix A. It was decided to use a patient with a moderate slip, because for these patients the in-situ fixation is the most common type of treatment. For very severe slips other surgical techniques, such as the modified Dunn procedure, might be needed to restore the femur geometry [35]. The influence of screw position on the expected growth pattern would therefore be less relevant for that particular SCFE patient group.

2.2.2 FE model

The steps for segmentation, generation of the growth plate, meshing and material assignment were the same as those described in the healthy growth modelling method. The segmentation and meshing parameters can be found in Appendix D. The MIMICS method was used for the generation of the growth plate. Although the results of the two growth plate generation methods as described in section 3.1 did not show large differences, it was decided to use the MIMICS method for the SCFE part of the study. The main reason was the smoother surface of the growth plate. Since thermal expansion was used in this part of the study, a smoother surface was assumed to generate more accurate results. Furthermore, the smoother surface makes it easier to visualise the amount of expected growth on the surface of the growth plate. The ring with the elements added to the growth plate region in ABAQUS later on is included in the plots in the results section for completeness, but the results on these elements are not discussed specifically as the inability to expand smoothly is believed to lead to inaccurate results in this region. The volumetric mesh of the growth plate within the femur can be seen in Figure 11.
The Hounsfield Unit (HU) values on the CT scan images were related to the density and elastic modulus of elements in the mesh, as described in section 2.1.6. On the CT scan image of the SCFE patient, the average HU value for air was -1024 HU and for cortical bone was 818.9 HU. Using the known density values for air and cortical bone, α and β were found to be 0.500626 and 0.000488, respectively, for this CT scan, using equation 1. The CT scan included the screw that was placed during in-situ fixation of the SCFE femur. To create a SCFE FE model that could be used for modelling the effect of different screw positions on growth, this original screw had to be removed from the FE model. The elements of the mesh in the region of the original screw could not be assigned material properties using HU values because of the presence of the screw. The HU value

in this region was hence estimated creating a mask right next to the original screw and computing the average HU value in this region. This value was used to assign appropriate density and elastic modulus values in the region of the original screw.



Figure 11: The creation of the volume mesh, with a growth plate that falls completely within the outer surface of the femur.

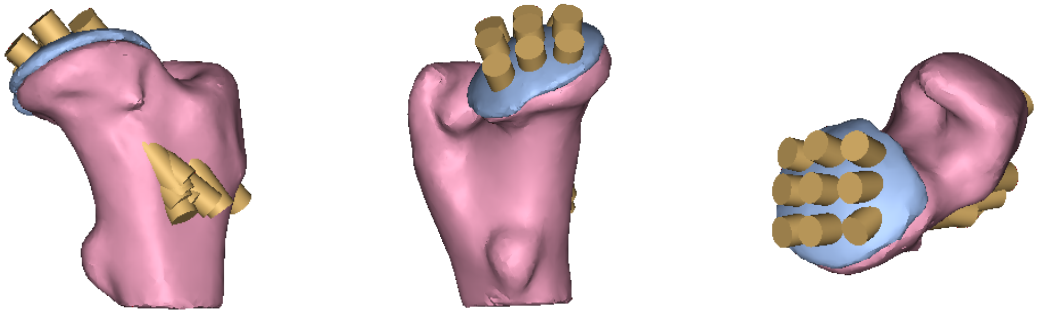
2.2.3 SCFE screws

In the process of fixation of SCFE, a fully or partially threaded screw of either 316L stainless steel or a standard titanium alloy is used [36, 37]. The patient used for this study received a Synthes fully threaded cannulated 6.5 mm screw. The screw has a 4.8 mm diameter shaft and a 6.5 mm diameter across the threads and is made of a titanium alloy (Ti-Al-7Nb). This titanium alloy has a Young's modulus of $100-110$ GPa and a Poisson's ratio of $0.35-0.37$ [38]. For this study a Young's modulus of $E = 105$ GPa $= 105000$ MPa and a Poisson's ratio of $v = 0.36$ were used for the screw. The aim for the surgeon is to place the screw such that at least four threads are in the physis and two on the femoral head side of the physis. This was demonstrated to be sufficient to avoid slip progression [9]. The screw itself is not applied with pretension, such that no compressive force is applied. However, as the physis still tries to grow, the bone will eventually apply compressive forces on the screw, and vice versa.
Surgeons often use a fully threaded screw, such that sliding contact between bone and screw is not possible. A study by [39] studied three different ways to model threaded screws in a finite element analysis: using a threaded screw, using a simplified geometry screw with the bone-screw interface modelled as uniformly tied (perfectly bonded) and using a simplified geometry screw with the bone-screw interface modelled as a cohesive-frictional interface. They found that both simplified configurations can be used to model a threaded screw. The study concluded that although the cohesive-frictional interface replicated principal strain distributions and magnitudes more accurately

than the perfectly bonded interface, the results of their study (comparing implant stability) were not affected by the modelling choice for the bone-screw interface and the perfectly bonded interface could therefore be a more efficient methodology due to its simplicity. Hence, in this study the screw was modelled as a cylinder that is perfectly bonded with the bone. All elements are connected such that the model consists of one part. A cylinder diameter of 6.5 mm was chosen, to match the diameter of the threads in the Synthes screws.

2.2.4 Locations of the screws

After the creation of the FE model, the different screw positions were added in ABAQUS using *getByBoundingCylinder* in a Python script, creating nine different models. The different positions were chosen to investigate the effect of placing the screw more anteriorly (A), posteriorly (P), medially (M) or laterally (L). In addition, placement of the screw in an anteromedial (AM), anterolateral (AL), posteromedial (PM) and posterolateral (PL) position were investigated to gain a more thorough understanding of the best location for screw placement. The coordinates of the screw in different positions were found using the CAD Tools in Mimics, which were used to create the cylindrical screw in ABAQUS. The nine screw positions used for the analysis are visualised in Figure 12.



(a) (b) (c)

Figure 12: The nine positions of the screw in the growth plate in the a) coronal and b) sagittal and c) axial view. The femoral head is hidden such that the position of the different screw configurations can be seen in the growth plate.

2.2.5 SCFE loading and boundary conditions

In SCFE, the epiphysis (femoral head) and the physis (growth plate) usually shift posteroinferior relative to the metaphysis [40], leading to retroversion [41]. The study by [40] investigated the effect of loading direction on the amount of slip of the physis and concluded that more varus loading conditions lead to increased physis shear. Combined with increased body weight and retroversion of the femoral head, this loading condition may lead to exceeding the ultimate yield point in the

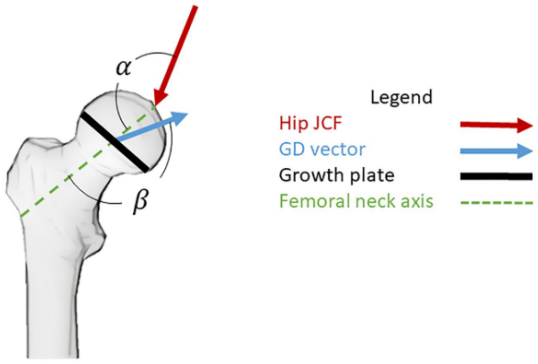
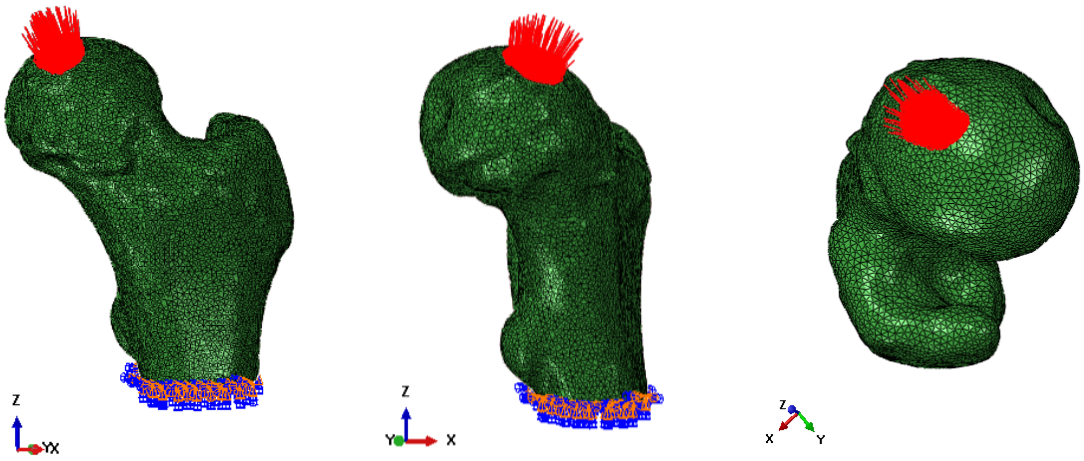


Figure 13: Schematic illustration of the application of the hip joint contact force (HJCF) on the femur, as applied by [34]. Angle α represents the angle between the HJCF and the femoral neck axis. Source: [34].

physis and hence result in a slip of the physis. It was also found that SCFE leads to a reduced contact area on the femoral head with the cumulative femoral contact area significantly smaller in severe SCFE cases compared to mild cases and that severe slips ($> 60°$) have higher peak and mean contact stress than mild slips ($< 30°$) [42].

It is generally acknowledged that the femoral head and the physis slip relative to the metaphysis. The slip relative to the acetabulum, however, depends. In some (milder) cases, it is mostly the femoral head and physis moving relative to the acetabulum, with the rest of the femur remaining close to the original orientation. In more severe cases, however, not only the femoral head and physis, but also the rest of the femur change orientation relative to the acetabulum. For the SCFE analysis, which uses a femur with a moderate slip (Southwick slip angle of 35°) [43], it is assumed that the femoral head and physis slipped, but the rest of the femur stayed in place relative to the acetabulum.

Most computational growth modelling studies modelled the load in the direction of the center of the femoral head, but in this study it is therefore more accurate to use a load orientation described relative to the femoral neck axis, as for instance done by [34] visualised in Figure 13. It was decided to use the same loading conditions as in the healthy growth study, but this time with the angles measured relative to a vertical line through the center of a disc in the femoral neck rather than relative to a vertical line through the femoral head center. In addition, the circular contact area has a diameter of 7.5 mm, such that it is half the size of the contact area in the healthy growth study to represent the reduced cumulative femoral contact area in SCFE. The applied load is shown in Figure 14. The same load was applied to all nine models representing the different screw orientations, since the focus of this study is on the effect of screw positioning on the areas of expected growth, rather than the effect of different applied loads.



(a) (b) (c)

Figure 14: The boundary conditions and the load applied to the femur in the a) coronal, b) sagittal and c) axial view. The load is applied with an inclination angle of 15° in the coronal plane, 20° in the sagittal plane and 35° in the axial plane, relative to the femoral neck axis. Method adjusted from [1] and [34].

2.2.6 Analysis

Different factors influence bone growth, as is visualised in Figure 15. The healthy growth study only included external mechanical loading (factor IIa) to be able to compare to the study by [1] and validate the FE model. For the slipped capital femoral epiphysis growth analysis, two distinct growth scenarios are analysed:

1. **Instant mechanical growth:** this case only considers growth due to external mechanical loading (factor IIa) and is calculated using the Osteogenic Index (OI), as explained in section 2.1.8. The results are presented in section 3.2.1.

2. **Long-term growth:** this case accounts for both biological growth (factor Ia) and bone-implant interaction (factor IIb) alongside external mechanical loading (factor IIa). The long-term growth results (biological, total mechanical and the combined growth) are given in section 3.2.3.

The first scenario shows the expected amount of *instant mechanical growth*. However, as bone growth takes place around the screw over time, the growth plate starts to exert forces on the screw and vice versa, introducing stresses in the growth plate. These stresses need to be added to the calculation for computing growth due to mechanical factors. In the second scenario, the biological growth (factor Ia) and bone-implant interaction (factor IIb) are therefore added to the SCFE analysis to visualise the *long-term growth*. Here the biological growth is modelled with thermal expansion of the growth plate and the bone-implant interaction is modelled through the stresses arising from this thermal expansion. For the long-term growth results, biological growth and mechanical growth are hence combined. The stresses arising from bone-implant interaction and

the stresses arising from the external load are summed for the effect of the total mechanical factors. Subsequently, the expected growth values from the biological factors and the total mechanical factors are exported from ABAQUS and post-processed in Python to obtain the combined growth results. The method for computing the combined growth is explained below. The results of the expected instant growth pattern due to mechanical factors can be found in section 3.2.1 and the long-term growth results (biological, total mechanical and the combined growth) are given in section 3.2.3. For the biological growth and the total mechanical growth the expected amount of growth (in mm/month) was furthermore calculated as the average growth value over all elements in the growth plate using a Python script. These values were used to plot the contribution of biological and mechanical factors to growth in the combined growth section.

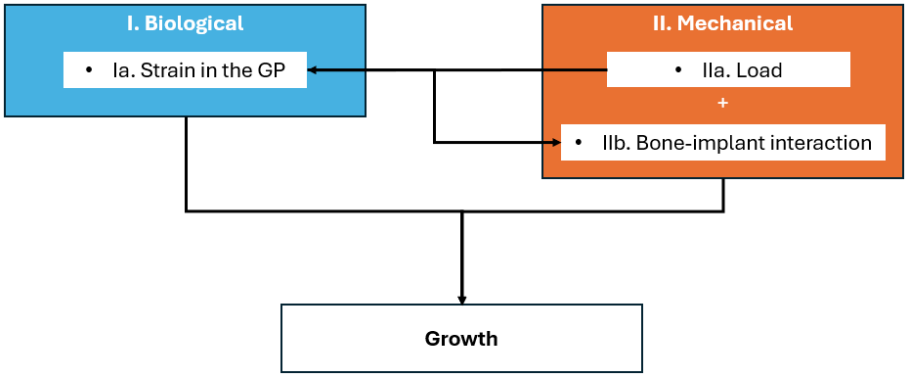


Figure 15: Factors influencing growth in the growth plate one month after placement of the screw.

Bone-implant interaction

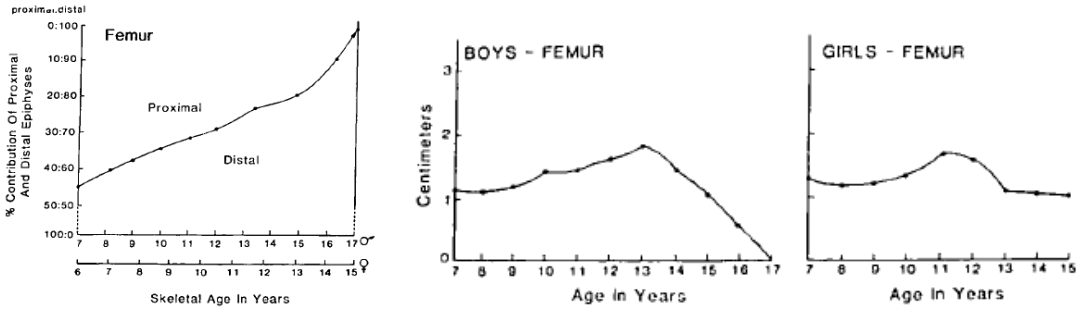
In order to model the bone-implant interaction, first a literature search was performed to investigate how bone-implant interaction is modelled in other studies. The aim was to either find force magnitudes or stress values that represent the interaction between the screw and the femur and could be added in the FE analysis or to find methods to simulate the bone-implant interaction ourselves. The results of this literature search can be found in section 3.2.2.

Sensitivity study

The Osteogenic Index (OI) is given in MPa and can be used to find and show regions of expected growth, but doesn't give a numerical value of expected amount of growth. Furthermore, many different values for the constants a and b in the OI formula are used in literature. To make the results easier to interpret for clinicians and to be able to compare results of this computational growth modelling study to clinical results, it was desired to express the expected growth in mm/month. In order to do so, a sensitivity study was performed to find the appropriate values for constants a and b in in formula 4 and for the thermal expansion coefficient α which is used to model biological growth. The sensitivity study is based on the amount of growth in the immature proximal femur as found in literature. Multiple studies into computational growth modelling of the femur use a growth rate of 9 mm/year in the proximal femur [21, 32], citing a study by Pritchet et al. (1992) [44]. For consistency and to be able to compare with those other studies, it was decided to also use this

growth factor of 9 mm/year, but it is important to note that this value is only applicable to a seven year old boy. The study by Pritchett et al. (1992) found that the values differ slightly between boys and girls, and that the growth rate decreases with age from 9 mm/year for boys and 8 mm/year for girls at age 7, to 0.65 mm/year for boys and 0.45 mm/year for girls at age 12 and eventually 0 mm/year for boys at age 17 and girls at age 15, as can be obtained from the graphs in Figure 16 [44].

Most studies use that the biological growth rate is twice the mechanical growth rate [32, 21], based on the findings of [45]. In that study avian embryos were paralysed completely in their first days of life, and the effect on bone growth was investigated. The researchers found that long bones exhibited up until 63% of their normal growth. From this finding it was concluded that bones grow roughly two thirds of their normal growth in the absence of mechanical loads, meaning that the magnitude of the biological growth is twice the magnitude of the mechanical growth. Hence, assuming total growth of 9 mm/year = 0.75 mm/month, the femur is expected to grow roughly 0.5 mm/month as a result of biological factors and 0.25 mm/month as a result of mechanical factors. Using the method proposed by [21] and the assumption that the mechanical contribution to bone growth is equal to half of the biological contribution of bone growth [45, 46], the biological growth rate can be computed and is found to be $\dot{\epsilon}_b = 0.167$ month^{-1} for a growth plate thickness of 3 mm. The full computation can be found in Appendix G. The strain values in the growth plate elements should hence be equal to $\epsilon_b = 0.167$ after one month of growth. This value, together with the 0.25 mm of expected mechanical growth after one month, is used for the parameter sensitivity analyses that were performed to find the appropriate thermal expansion coefficient α to represent one month of biological growth and the constants a and b in the osteogenic index formula to simulate one month of mechanical growth. Different a, b and α values were used for simulations and the expected amount of growth results were compared to these computed expected amounts of growth to find the values that represent an accurate amount of growth. The results of this sensitivity study can be found in section 3.2.2. The obtained values are used to compute the expected growth patterns due to mechanical and biological factors in the SCFE long-term study.



(a) (b)

Figure 16: The graphs show a) the contribution of the proximal and distal growth plates to growth of the femur and b) the annual growth of the distal femur in boys and girls from age seven to skeletal maturity. Source: Adapted from [44].

Combined growth

To get the total amount of expected growth, the total amount of growth as a result of mechanical factors and the amount of biological growth need to be combined. This gives the total expected growth in the femur, here called combined growth. Different methods exist to do so. The study by [47] for instance computes the total growth as a linear combination of the biological factor and the mechanical factor in the form of a cartilage maturation index (CMI) according to:

$$CMI = BG + d \cdot MG \tag{7}$$

where BG is the biological growth factor, MG the mechanobiological growth factor and d is the coefficient determining the ratio of the contribution of both. This CMI is used to determine the thermal expansion coefficient that is assigned to the elements in the growth plate according to

$$\dot{\epsilon} = G_{hm} \cdot CMI \tag{8}$$

where G_{hm} is a constant. Multiple other studies compute the *specific-growth rate* as the sum of a biological component $\dot{\epsilon}_b$ and a mechanical component $\dot{\epsilon}_m$ according to

$$\dot{\epsilon} = \dot{\epsilon}_b + \dot{\epsilon}_m \tag{9}$$

where $\dot{\epsilon}_m$ is calculated with the OI formula (according to equation 4) and $\dot{\epsilon}_b$ is taken as a constant [32, 31, 21]. A study by Rutten [33] used this method with a constant biological growth value of 0.36 mm/step, as also found in [32]. The study by Rutten simulated one month of growth per step. In every step the growth is computed according to formula 9, with $a = 0.02$ month^{-1} MPa^{-1} and $b = 0.01$ month^{-1} MPa^{-1} in the OI formula, equal to values used by [21].

In line with equations 8 and 9, in this study the *combined growth* was taken as the sum of the biological growth and the mechanical growth according to:

$$\text{combined growth} = BG + MG = t \cdot \epsilon_b + OI \tag{10}$$

where BG is the biological growth, MG the mechanical growth, t the thickness of the growth plate (in mm), ϵ_b the strain due to biological factors and OI the growth due to all mechanical factors (in mm).

Other studies sum the biological and mechanical growth, such that a negative OI value could eliminate a positive biological growth value. Negative specific-growth rates are then taken as zero, indicating no growth. The study by Sadeghian et al. (2021) furthermore only uses the CMI to grow elements for which the CMI exceeds a certain critical value CMI_{cr} (these elements are identified as part of the growth plate), which is evaluated in every iteration by the average and one standard deviation of the CMI over all cartilage elements [47], such that small growth values are not used to grow the growth plate. In this study, the external load was already taken into account when computing the biological growth, thereby reducing the amount of biological growth. Summing a negative value of the OI with the biological growth would introduce this effect again, leading to including this factor twice. Therefore, it was decided by the authors of this study to take negative OI values as zero before summing up the mechanical and biological contributions to growth.

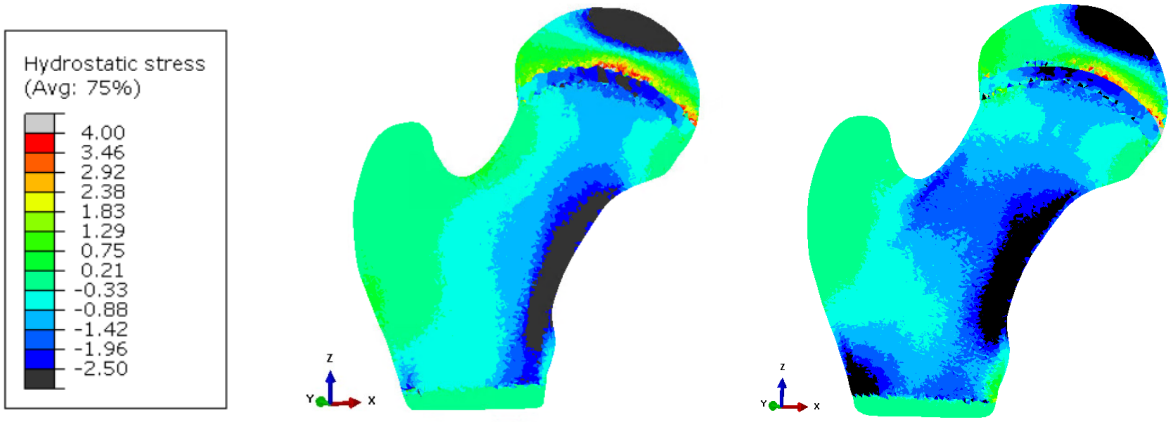
3 Results

3.1 Healthy femoral growth

The results of the healthy growth study are presented below, with a side-by-side comparison of the ABAQUS and MIMICS method for clarity. First the hydrostatic stress, octahedral shear stress and osteogenic index distribution across a cross section of the femur are shown, after which the values in the growth plate are presented.

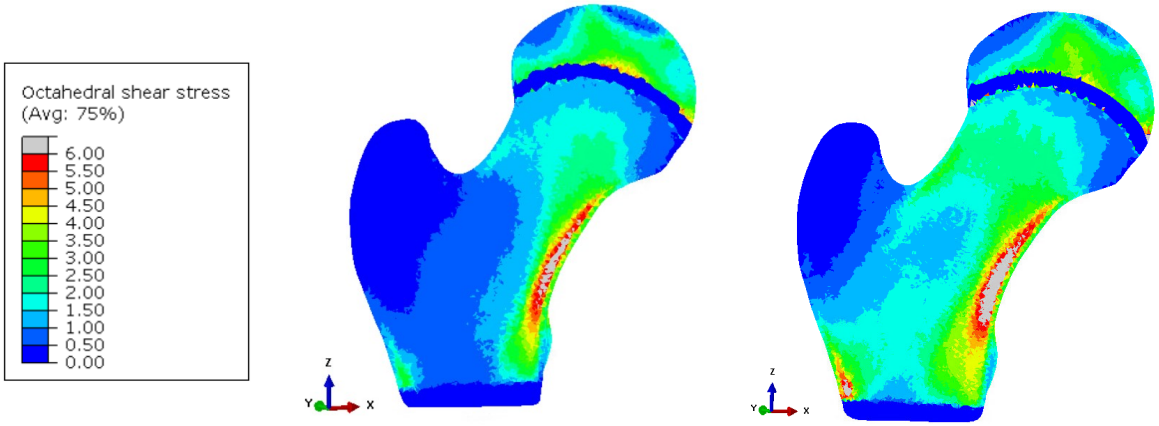
3.1.1 Stresses in the femur

The hydrostatic stress and the octahedral shear stress values in the femur as a result of the externally applied load are visualised in Figures 17 and 18 below. It can be observed that some small differences are present in the results of both methods. Overall, the stress pattern is similar, with the hydrostatic stress showing positive values above the growth plate (showing tension) and negative values underneath the growth plate (showing compression). The highest value occurs right on top of the growth plate at the location where the load is applied. The hydrostatic stress value is lowest at the surface at the location where the load is applied and at the inferior end of the femoral neck and shaft. However, with the MIMICS method, the hydrostatic stress values in the femoral neck are lower compared to the ABAQUS method. In both methods low values are observed on the medial side, but the MIMICS method also shows low values on the lateral side (approximately -2 MPa compared to roughly -0.33 MPa in the ABAQUS method).
The octahedral shear stress also has a similar stress pattern in both methods, with the highest values reached right above the growth plate in the center, and on the medial side of the femoral neck. However, the MIMICS method shows higher values in the neck compared to the ABAQUS method ($1.5 - 4$ MPa compared to $1 - 2.5$ MPa). The values in the femoral shaft are also slightly higher in the MIMICS method ($1.5 - 5$ MPa compared to $0.5 - 3$ MPa in the ABAQUS method).
The osteogenic index (OI) is the parameter used to predict growth in the femurand its distribution across a cross section of the femur is depicted in Figure 19. Although the applied load leads to high compression, and hence low OI values, at the surface area where it is applied, it leads to high OI values right above the growth plate, located underneath the load application area. This indicates growth at that location. Right above the growth plate the OI is furthermore slightly higher on the medial side than on the lateral side. Again, the overall pattern of the OI distribution is similar for both methods, but differences can be observed in the OI values in the neck and shaft, with the values being slightly higher in the MIMICS method.



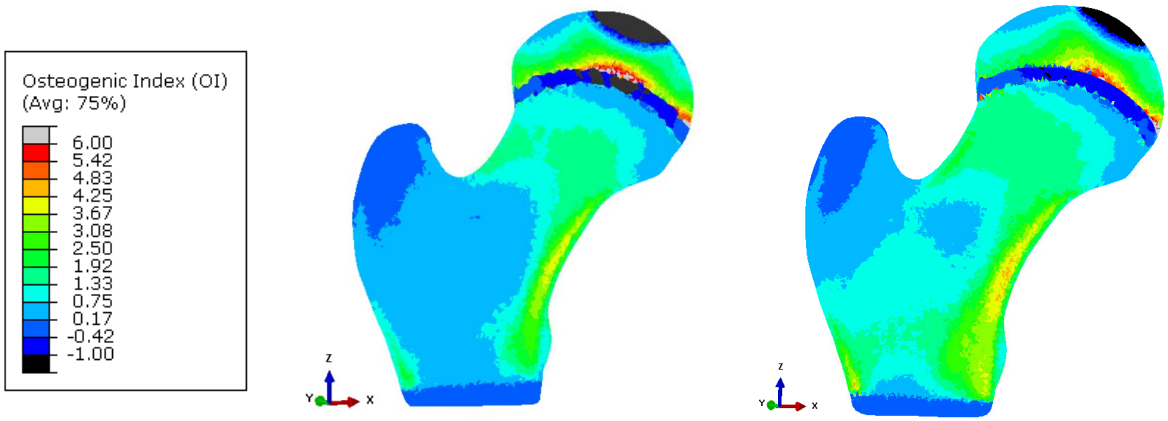
(a) (b)

Figure 17: The hydrostatic stress (in MPa) in a cross section of the femur using the a) ABAQUS method and the b) MIMICS method.



(a) (b)

Figure 18: The octahedral shear stress (in MPa) in a cross section of the femur using the a) ABAQUS method and the b) MIMICS method.

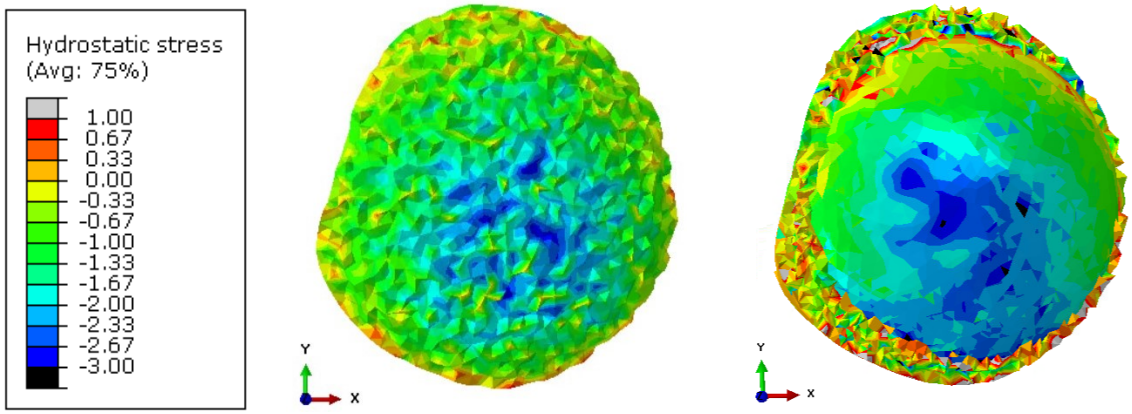


(a) (b)

Figure 19: The osteogenic index (in MPa) in a cross section of the femur using the a) ABAQUS method and the b) MIMICS method.

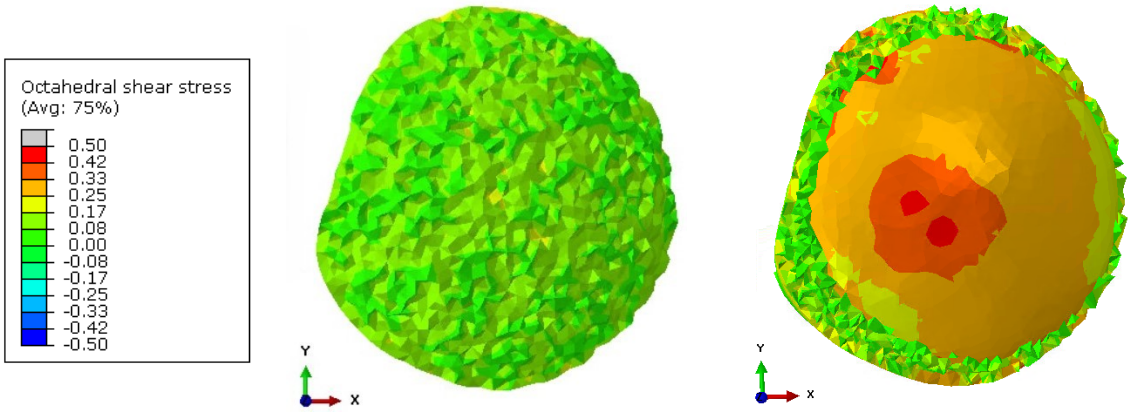
3.1.2 Stresses in the growth plate

The hydrostatic stress, octahedral shear stress and the osteogenic index in the growth plate are visualised in Figures 20, 21 and 22. The results obtained with the ABAQUS method and the MIMICS method are visualised next to each other such that they can be compared. Overall it can be observed that the results obtained with the MIMICS method are much smoother than the results obtained with the ABAQUS method. Only the outer ring of the growth plate in the MIMICS method, which was added later on and not taken into account during meshing, is not smooth. Some of these rough edge elements show high stress values. This is not observed in the plots of the ABAQUS method. The hydrostatic stress results are similar for both methods. The highest compressive stresses (around -3 MPa) can be observed in the center of the growth plate, slightly more towards the anterior side. The highest tensile stresses are seen on the edges in both methods, but the values are slightly higher in the MIMICS method (about 1 MPa in the MIMICS method compared to 0.33 MPa in the ABAQUS method). The octahedral shear stress results do show large differences between both methods with values close to 0 MPa throughout the growth plate for the ABAQUS method and values up to approximately 0.42 MPa in the MIMICS method, with the highest value occurring the center of the growth plate, slightly toward the anterolateral side. The osteogenic index results are similar in both methods with the lowest values around -1.2 MPa in the center and on the anterior side and the highest values at the edges (approximately 0.3 MPa for the ABAQUS method and 0.8 MPa for the MIMICS method). The finding that the largest differences in results between both methods are observed in the octahedral shear stress are in line with the findings of [1]. Additionally, the stress peaks at the edges of the growth plate, observed when the segmentation is performed in MIMICS but not when the segmentation is performed in ABAQUS, were also reported by Roels et al. [1].



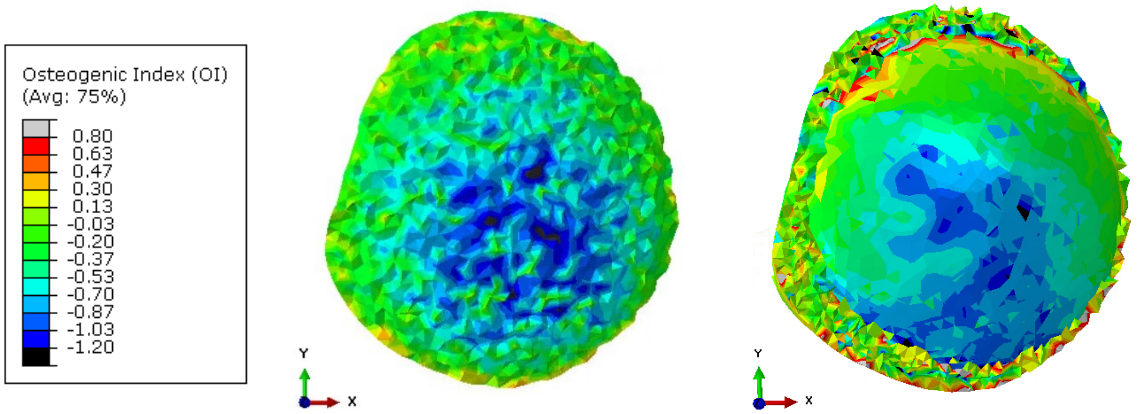
(a) (b)

Figure 20: The hydrostatic stress in the growth plate (in MPa) using the a) ABAQUS method and the b) MIMICS method.



(a) (b)

Figure 21: The octahedral shear stress in the growth plate (in MPa) using the a) ABAQUS method and the b) MIMICS method.

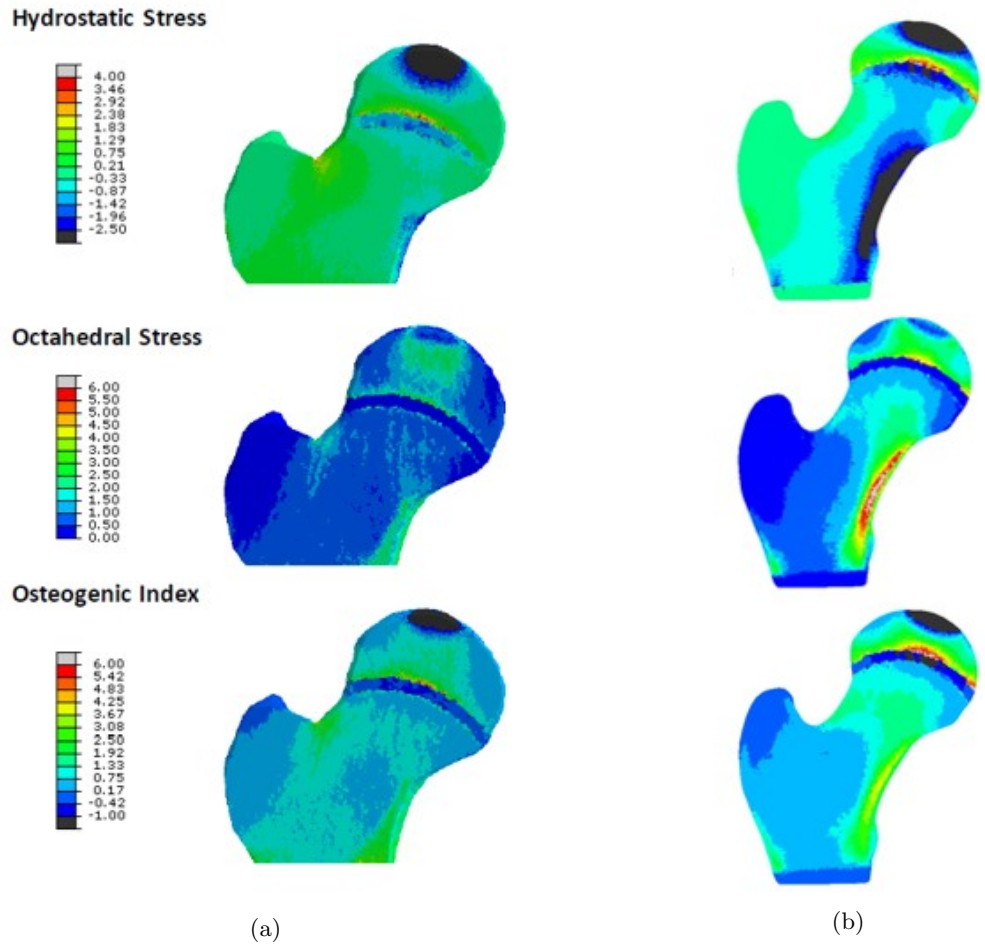


(a) (b)

Figure 22: The osteogenic index in the growth plate (in MPa) using the a) ABAQUS method and the b) MIMICS method.

3.1.3 Comparison to Roels et al. [1]

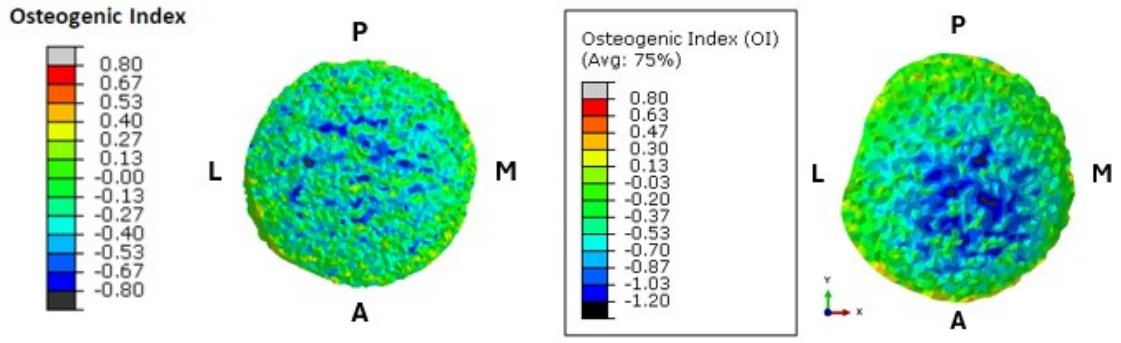
The results of the healthy growth study are compared to the results of the study by Roels et al [1], which is visualised in Figures 23 and 24 in the whole femur and in the growth plate, respectively. The study by Roels et al. found that the results of the MIMICS method were much smoother than the results of the ABAQUS method. They observed the largest differences between both methods in the octahedral shear stresses, which were slightly higher in the MIMICS case, leading to higher OI values. Both of these findings are in accordance with the findings in this study. Although the authors of the study by [1] concluded that the plots of the MIMICS method provided a more distinct pattern in the growth plate, the ABAQUS method was used for the FE analysis of the different load cases in that study. It is not explained why that is the case, but it is likely due to the ABAQUS method being much easier to implement, as mentioned in their discussion. Therefore, the results of the ABAQUS method of this study are compared to the results of their normal load case (also created with the ABAQUS method).
The results of both studies visualised on the whole femur are shown in Figures 23a and 23b. The overall stress patterns are similar in both studies. However, small differences in the stress pattern can be observed in the femoral neck. In the the study by [1] the stress pattern is relatively uniform in the femoral neck and greater trochanter, whereas in this study lower hydrostatic stress values and higher octahedral shear stress values can be observed in the neck compared to the area of the greater trochanter. The order of magnitude of the stresses is also similar in the results of both studies. However, the magnitude of the stresses is higher in this study than in the study by [1]. This is mostly seen in the femoral neck and shaft, which reach OI values ranging from $0.75 - 4.25$ MPa in this study compared to $0.17 - 2.50$ MPa in the study by Roels et al. It is important to note the difference in weight of the patients in both studies. Both studies use an external load of 250% body weight to represent the hip contact force, but in the study by [1] that resulted in a peak force of 1200 N, whereas this study used a peak force of 1925 N. Additionally, it should be noted that there are geometrical differences between the femurs used in both studies. The neck of the femur used in this study is longer and thinner than the neck of the femur used in the study by [1]. The FE model used in this study also includes a larger proportion of the femoral shaft than the study by [1].



(a) (b)

Figure 23: Stresses in the femur under normal loading in a) the study by Roels et al. Source: [1] and b) this study using the ABAQUS method.

The results of both studies visualised on the growth plate are shown in Figures 24a and 24b. In the figures, the medial (M), lateral (L), anterior (A), and posterior (P) sides of the growth plate are added to indicate the anatomical orientation. The osteogenic index plotted on the GP for the normal load case is compared. It can be observed that the order of magnitude of the OI is similar in both studies, with values ranging from -80 MPa to 0.40 MPa, but the stress distribution is slightly different. In the study by [1] the lowest OI values are observed in the center, slightly more towards the posterior side, whereas in this study the lowest OI values are also found in the center, but shifted more towards the anterior side of the growth plate. Furthermore, the region with the lowest OI value is slightly larger in the results of this study. In both studies the highest OI values are observed on the edges of the growth plate.



(a) (b)

Figure 24: Stresses in the growth plate under normal loading in a) the study by Roels et al. Source: [1] and b) this study using the ABAQUS method.

3.1.4 Comparison to CT scan data

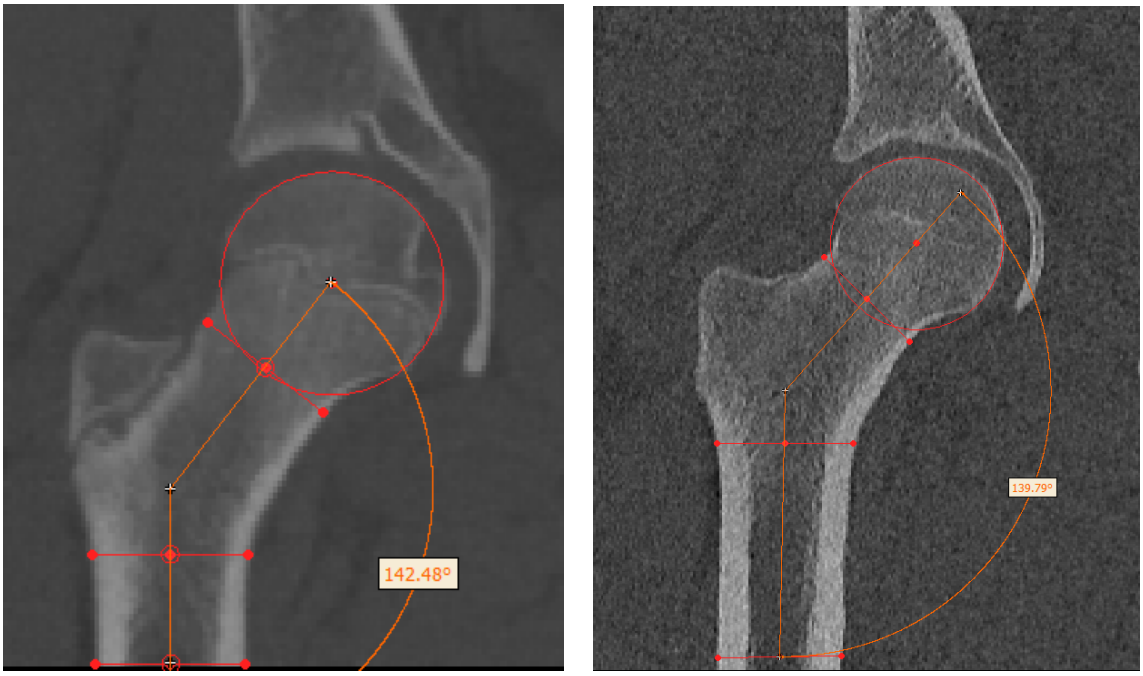
In addition to the comparison of the FE analysis results to those of Roels et al. [1], the results are compared to the change in the neck-shaft angle measured on the baseline and follow-up CT scans of the healthy growth patient. Table 2 shows the angles measured on the CT scans of the healthy growth patient at baseline and at the follow-up scan taken 30 months later. These angles are used to compare the expected areas of growth (in the form of the OI results) in the femur and growth plate to the actual growth and change in geometry in the femur of the healthy growth patient.

Measurement	Baseline scan	Follow-up scan
Neck shaft angle	142.48°	139.79°

Table 2: Measured angles in the CT scans at baseline and at 30 months follow-up. The growth plate was still open at the follow-up scan.

Neck shaft angle (NSA)

The neck-shaft angle (NSA) is defined as the angle between the femoral neck axis (FNA) and the femoral shaft axis (FSA), but there exist various different methods to measure these axes [48]. Furthermore, femoral rotation influences the measurement of the NSA on AP radiographs. In this study, the FNA is obtained from the coronal view of the CT scans (matching the view of AP radiographs) by drawing a line between the centre of a circle fitted to the femoral head and the midpoint of the femoral neck's smallest diameter. The FSA is obtained by the midpoint of the femur's diameter 1 cm under the lesser trochanter and at the bottom of the radiograph. The measurements of the NSA in the baseline and follow-up CT scan are shown in Figure 25. This decrease in NSA over time is in agreement with the results of a study by [49], which included 312 femurs (24 limbs per year for each age) and found that the NSA changes from 138.49° at 4 years old to 129.19° at 16 years old using this "circle fitting" method to compute the NSA [49].



(a) (b)

Figure 25: The circle fitting method by [49] applied to measure the NSA in the a) baseline scan and b) follow-up scan of the healthy patient.

This clinically observed decrease in NSA angle of the healthy growth patient is not in accordance with the OI results of the healthy growth study, which show more expected growth on the medial side right above the proximal femoral growth plate than on the lateral side. Growth on the medial side above the growth plate would lead to a superolateral shift of the femoral head center, which would cause an increase in NSA angle.

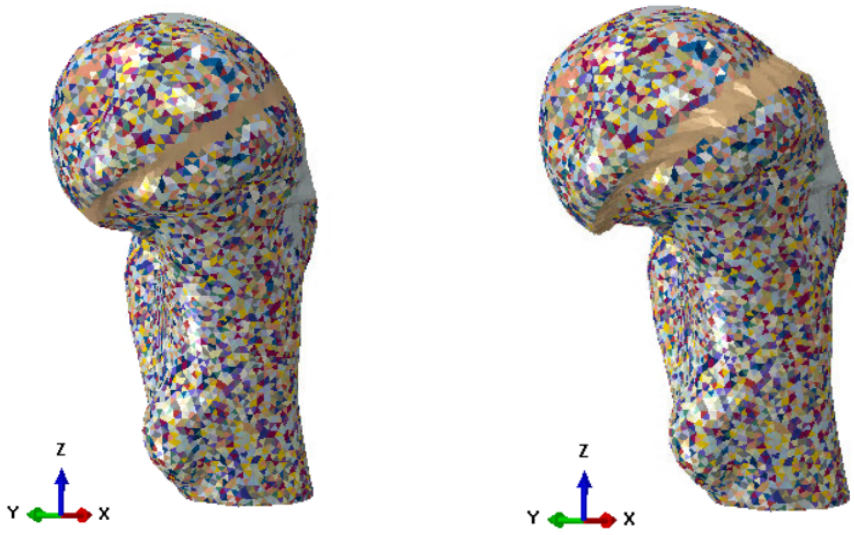
3.2 SCFE femoral growth

3.2.1 Instant mechanical growth (external load only)

This chapter shows the results of the SCFE analysis for growth right after surgery. At this stage the growth plate grows as a result of biological and mechanical factors, as explained in section 2.1.8 and shown in Figure 10. In this first analysis only the mechanical factors (IIa in Figure 10) are included, consistent with the study by [1], to see how the different screw positions influence the stresses in the growth plate and hence the mechanical factors contributing to bone growth.

Displacement

First, the external load is applied on the femur with no screw to look at the effect of this load on (further) slipping of the femoral head. Figure 26a and 26b show the femur before and after application of the load. Without placement of a screw the femoral head slips further in posteroinferior direction, showing the necessity of in-situ fixation.



(a) (b)

Figure 26: The displacement of the femoral head in the case with no screw. A scale factor of 5 is used to visualise the slip. The material view is used for clarity, with the beige area representing the growth plate.

Stresses

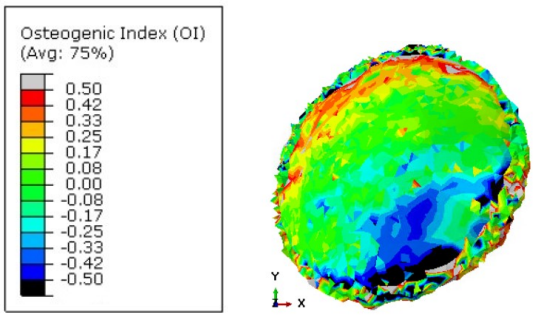
The results of the expected growth pattern due to mechanical factors for the different screw positions instantly after surgery are shown in Figure 28. At this stage the screw does not exert forces on the growth plate yet. It can be observed in Figures 28a and 28f that with the screw in the anterior and anterolateral position, the osteogenic index value in the area of the externally applied load is less negative than in the other configurations. This shows that the screw takes some of the

load applied on the femur, rather than the load being transferred through the growth plate. The reduced compressive stresses in the area of the externally applied load lead to lower hydrostatic stresses and an osteogenic index value closer to zero in the area of the externally applied load. This is in accordance with the results of a previously performed study by Hucke et al. [50]. However, in the configurations where the screw is not close to the external load position, the OI values are much lower than in the case without a screw.

In addition, it can be observed that positive osteogenic index values can arise on the contralateral side of the externally applied load. The externally applied load leads to compressive stresses, but also introduces tensile stresses on the opposite side of the growth plate. When the screw does not take away the compressive stresses in the growth plate induced by the externally applied load, these tensile stresses arise and stimulate bone growth, as can be seen in the configurations with the screw in medial, anteromedial, posteromedial and posterolateral position. With the externally applied load on the anteromedial side of the growth plate, the growth is stimulated on the lateral side of the growth plate for the medial and anteromedial screw positions, as can be seen in Figures 28c and 28e. The screw in the posteromedial position stimulates growth on the posterolateral side of the growth plate, as can be seen in Figure 28g and the screw in posterolateral position stimulates growth on the posteromedial side of the growth plate, as can be seen in Figure 28h. In the anterior, lateral, anterolateral and middle screw locations it can be observed that the screw is carrying most of the externally applied load, such that smaller compressive stresses and therefore no tensile stresses arise in the growth plate. In these configurations bone growth is not stimulated and no growth will happen as a result of the externally applied load.

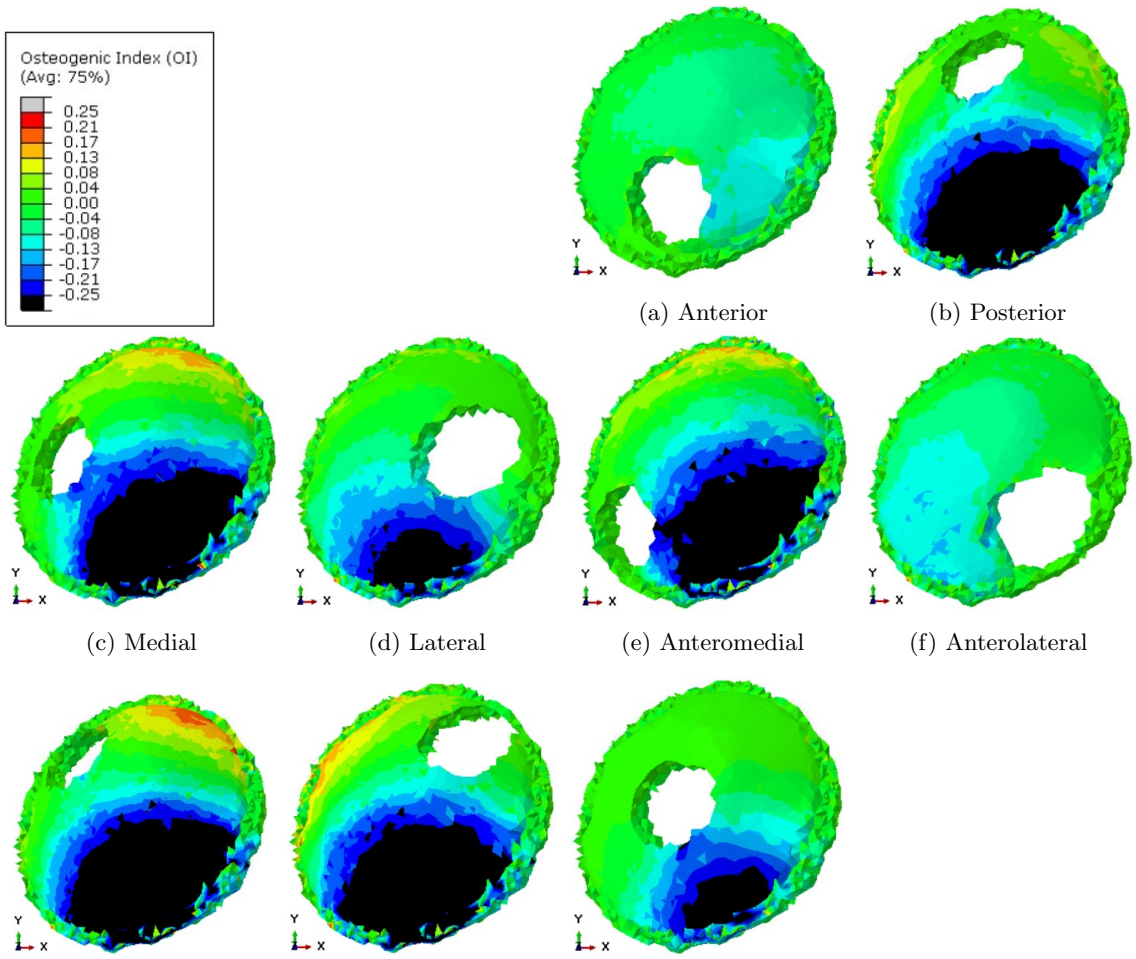
In slipped capital femoral epiphysis the femur head slips in posterior and inferior direction. Therefore growth on the posterior side of the growth plate is desired such that the growth plate grows in superior direction on the posterior side and the femur head center will shift slightly back to the anterior side. Looking at initial growth immediately after surgery and only taking into account the influence of the externally applied mechanical load on bone growth, the medial, anteromedial and posteromedial positions of the screw would hence be most beneficial.

Osteogenic Index



(a) No screw

Figure 27: The osteogenic index (OI) in the growth plate in the case with no screw.



(a) Anterior (b) Posterior

(c) Medial (d) Lateral (e) Anteromedial (f) Anterolateral

(g) Posteromedial (h) Posterolateral (i) Middle

Figure 28: The osteogenic index in the growth plate for different screw positions. The screw elements are removed for visualisation purposes. A visual of the screw positions is given in Figure 12.

3.2.2 Sensitivity study

When an implant has been in the bone for some time, the bone and the implant start to exert forces onto each other. This chapter discusses this phenomenon by first going into what is currently known from literature and then showing the results of the parameter sensitivity analysis.

Bone-implant interaction in literature

As the femur grows from the growth plate, it starts to exert a force on the implant and there is a reaction force from the implant on the bone and cartilage. In 2018, a study by Schneider et al. stated that the loading conditions of implants induced by the physis were not known [51]. They claimed to be the first study to utilise FE simulations to predict the forces arising in modulated growth. They performed FE simulations on a simplified version of the juvenile distal femur with an Eight-Plate implant system (Orthofix Inc., Lewisville, TX) often used to treat varus-valgus deformities (VVD). The aim was to predict reaction forces by reproducing the screw deformation visible on radiographs of clinical cases with the FE model. They found that the possible range for the vertical reaction force of the screw on the femur F_g was between $129 - 580$ N for the simulated VVD treatment with an Eight-Plate implant. The authors then estimated the average stress in the physis by normalising this reaction force to half of the physis area, assuming that in VVD this implant acts on one half of the growth plate [52], as a stress between

$$\sigma = F/A = 129/(1360 \cdot 10^{-6}) = 0.09 \text{ MPa} \tag{11}$$

and

$$\sigma = F/A = 580/(1360 \cdot 10^{-6}) = 0.43 \text{ MPa} \tag{12}$$

in the growth plate in the area affected by the implant. A more detailed explanation of the methodology used by Schneider et al. is given in Appendix F.1.

The study by Alonso et al. (2022) investigated the interaction between bone longitudinal growth and an orthotic epiphyseal stapling device (a Blount staple) in the distal femur in the form of a 2D model. They investigated the *growth pressure* (the stress tensor component) around the staple and found that a compressive load appears between the staple legs, while a tensile load emerges in the diaphyseal zone next to the staple, promoting bone growth [53]. A figure of this finding is given in Appendix F.2.

The study by Hucke et al. (2023) performed a similar study with a tension-band implant at the tibio-femoral joint [50]. The authors investigated how the implant influences the mechanical loading of the growth plate. Results indicated that the implant leads to reduced growth rates in the insertion region, whereas the growth rate increases on the contralateral side of the growth plate, due to increased tension [50]. A figure of the growth rate results can be found in Appendix F.3. An interesting observation was that right after placing the implant, a reduction of the absolute stress values on the implant side was observed, while the overall pattern of stress distribution remained similar. This is in accordance with the SCFE instant growth results of this study, where it was observed that the screw could carry some of the compressive load for certain screw positions, as can be seen in Figures 28a and 28f for the anterior and anterolateral screw positions. At the end of treatment, when the implant had been present for a while and the growth plate cartilage had had time to grow, high pressure (static compressive stresses) and shear stresses were observed in the area

of the implant. The higher the implant force, the higher the increase in static pressure stresses and the larger the influenced area was (i.e. after a longer period of time, and more biological growth, the compressive stresses around the implant were higher and occurred in a larger region around the implant). In addition, the tensile stresses in the lateral half of the GP, opposite the anteromedial implant, were increased.

These previous studies show that not only the external load on the bone influences mechanical bone growth, but also the stresses induced by the bone-implant interaction. These factors should be combined to accurately model bone growth as a result of mechanical factors. However, although these studies looked into bone-implant interaction and the stresses arising around the implant, none of those studies looked into screws placed across the physis as done in in-situ fixation of SCFE. The setup of the studies described was too dissimilar from in-situ fixation of SCFE to directly translate the results to forces or stresses arising around a screw in in-situ fixation of SCFE and incorporate those in the FE analysis of this study. It was therefore decided to model the bone-implant interaction and stresses around the screw using an FE model with thermal expansion of the growth plate elements. Biological growth is thus used to find the stresses occurring because of bone-implant interaction. Literature was searched to find which values for the thermal expansion coefficient α and temperature change ΔT were suitable to use in ABAQUS to simulate biological growth in the growth plate. The results of this are shown in Table 3. The studies by Sadeghian et al. [54], Yadav et al. [21] and Carriero et al. [32] used thermal expansion in the last step after computing the combined growth as an output to grow the model and then update the nodal coordinates, rather than using it for biological growth as an input to compute the stresses in the growth plate as desired in this study to find the bone-implant interaction stresses. In addition, a wide variety of values was used for the thermal expansion coefficient α and the temperature change ΔT in the studies and no consensus was found in literature for suitable values to represent biological growth. To find an appropriate value for the thermal expansion coefficient of the growth plate elements, a sensitivity study was therefore performed. Next to this biological parameter sensitivity study to find the suitable thermal expansion coefficient α, a mechanical parameter sensitivity study was performed to find values for a and b in the OI formula (formula 4) such that the growth is expressed in mm/month. These results of these sensitivity studies are presented in the next section.

Study	**Thermal expansion coefficients α**	**Temperature change applied ΔT**	**Simulated growth time**
Sadeghian et al. (2023) [54]	Equal to growth rate: $CMI = BG + 0.2 \cdot MG$	$\Delta T = 1$	One gait cycle
Yadav et al. (2016) [21]	$\alpha_{xx} = 1$ $\alpha_{yy} = \alpha_{zz} = 0$	Temperature equal to the obtained growth rate $\dot{\epsilon}$	1 month (for 1 step in the simulation)
Schneider et al. (2018) [51]	$\alpha_{xx} = \alpha_{yy} = 0$, $\alpha_{zz} = 0.01$	ΔT varied in the study $\Delta T = 150K$ was most accurate (to simulate avg. 224 days of growth)	224 days
Carriero et al. (2011) [32]	Not mentioned	Specific growth rate $\dot{\epsilon} = \dot{\epsilon_b} + \dot{\epsilon_m}$ taken as the temperature	-

Table 3: Thermal expansion values used in other papers, with α_{xx} the mediolateral, α_{yy} the anteroposterior and α_{zz} the craniocaudal (growth plate direction of growth) directions.

Parameter sensitivity study

This section contains the results of the sensitivity studies performed to find the values for a and b in formula 4 and for the expansion coefficient α of the growth plate material in the finite element model that correspond to expected growth values due to mechanical and biological factors, respectively. The parameter sensitivity study is based on the amount of growth in the immature proximal femur as found in a longitudinal growth study in children by [41], which was explained in section 2.2.6 of the methodology. The subsections below show the expected amounts of growth in the growth plate for different a, b and α values, which are compared to the desired strain values in the growth plate elements of $\epsilon_b = 0.167$ after one month of only biological growth and 0.25 mm of expected mechanical growth after one month.

Mechanical: a and b values

Many different values for a and b in formula 4 are used in literature. The study by [33] uses a similar load case as used in this study and uses values of $a = 0.02$ month^{-1}MPa^{-1} and $b = 0.01$ month^{-1}MPa^{-1}. The study by [32] uses values of $a = 0.02$ days^{-1}MPa^{-1} and $b = 0.02$ days^{-1}MPa^{-1}. The study by [31] uses $a = 6$ days^{-1}MPa^{-1} and $b = 3$ days^{-1}MPa^{-1}. Other studies only model the octahedral shear stress and the hydrostatic stress, but not the osteogenic index [50], or only use the hydrostatic stress to compute the mechanical stimulus to growth [53]. These studies hence do not use a and b values. As discussed before, the ratio b/a should be between 0.3 and 1 to predict accurate endochondral ossification patterns [27], and is often chosen to be $b/a = 0.5$ in the osteogenic index formula [21, 32, 33, 1, 31]. To express the osteogenic index in expected millimeters of growth per month, the constants a and b are determined using a sensitivity study. The ratio is kept at $b/a = 0.5$, but different combinations of values are tested. The osteogenic index values for the different a and b values are exported from ABAQUS and a simple Python script was written to compute the average OI values for the different a and b values and plot the results. The result of this can be seen in Figure 29. It can be observed that the most accurate a and b

values to simulate one month of mechanical growth in the femur are $a = 0.5$ mm month^{-1}MPa^{-1} and $b = 0.25$ mm month^{-1}MPa^{-1}.

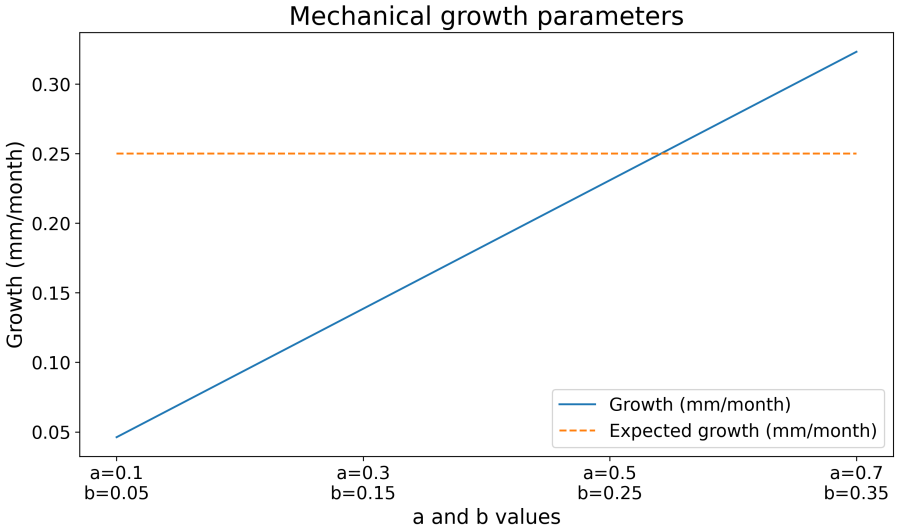


Figure 29: The expected amount of growth (in mm/month) in the growth plate as a result of mechanical factors.

Biological: thermal expansion coefficient

The thermal strain is calculated according to

$$\epsilon = \alpha \cdot \Delta T \tag{13}$$

such that the thermal strain ϵ follows a linear relationship with the thermal expansion coefficient α. Different combinations of α and ΔT are possible to simulate biological bone growth. For this study it was decided to use $\Delta T = 1$ K and to vary α_z in the parameter sensitivity analysis to obtain the most accurate thermal expansion coefficient α_z value to simulate one month of biological growth. The expansion coefficients in x- and y-direction are set to zero, as also done in [31]. Strain is calculated according to

$$\epsilon = \frac{\Delta L}{L_0} \tag{14}$$

Hence, for expected biological growth of 0.5 mm/month, the expected strain for a growth plate of 3 mm is

$$\epsilon = \frac{\Delta L}{L_0} = \frac{0.5 \text{ mm}}{3 \text{ mm}} = 0.167 \tag{15}$$

after 1 month of growth due to biological factors. The full computation of the biological growth can be found in Appendix G. For this analysis the model without screw without the externally applied load is used, because the assumption of the biological growth being approximately two thirds of the total growth originates from a study in which there were no mechanical loads at all [45]. The strain values of the elements of the growth plate for the different thermal expansion coefficient values are

exported from ABAQUS and a simple Python script is used to compute the average strain values in the growth plate for the different thermal expansion coefficient values and plot the results. The result of this can be seen in Figure 30. It can be observed that using these material properties and a temperature difference of $\Delta T = 1$ K, the most accurate thermal expansion coefficient to simulate one month of biological growth in the proximal growth plate of the femur is $\alpha = 0.2$ K^{-1}. To give an idea, the expected amount of growth after 6 months is also given. It can be observed that to simulate 6 months of growth, a value of $\alpha = 1.35$ K^{-1} would have to be used.

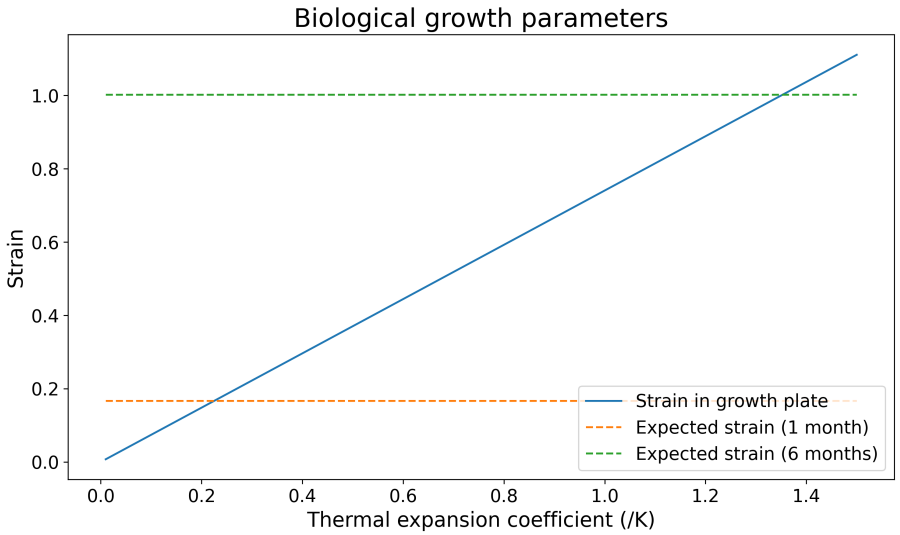


Figure 30: The expected amount of strain in the growth plate after 1 and 6 months and the observed amount of strain for different thermal expansion coefficient values.

3.2.3 Long-term growth

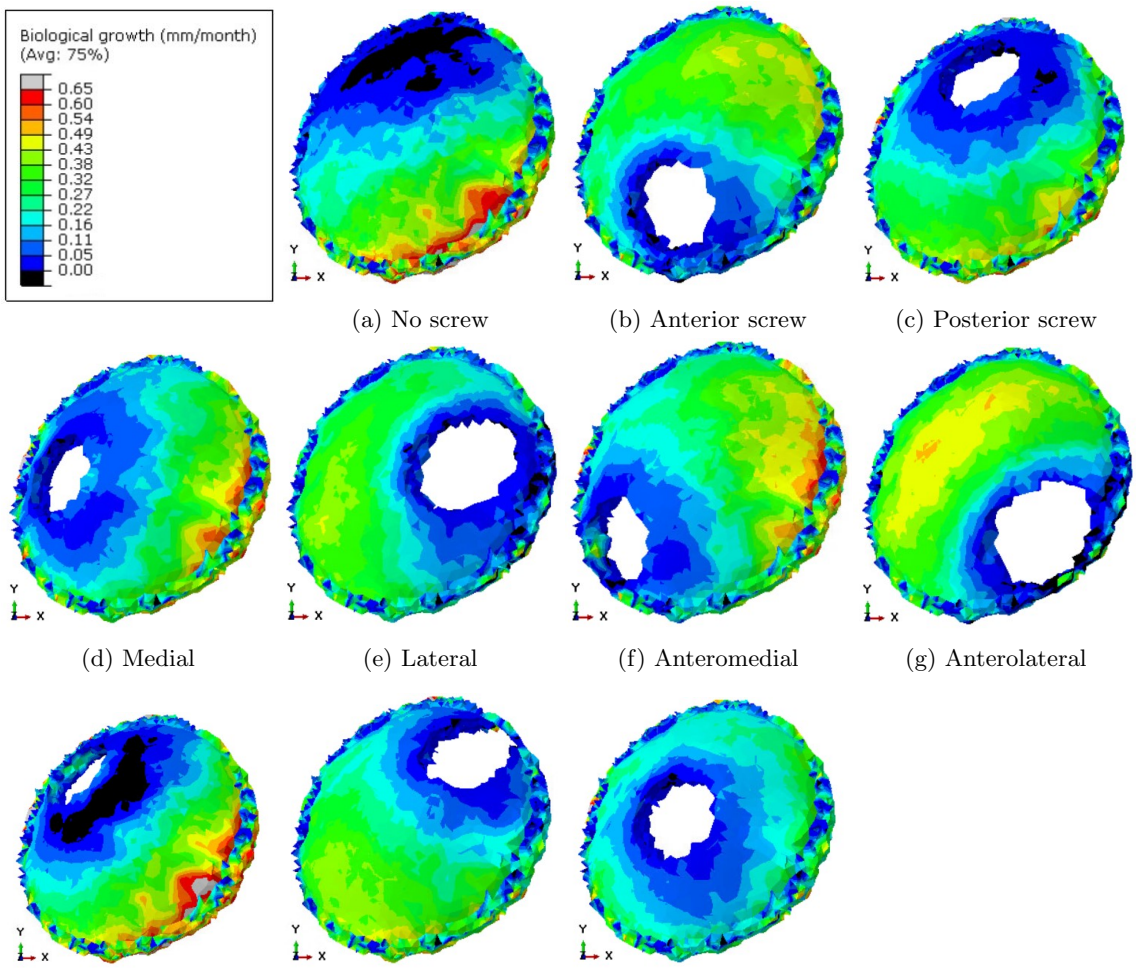
The results in Figures 27 and 28 show the expected growth in the growth plate due to external forces. In that analysis the stresses (mechanical factors) exerted by the implant on the bone are not included, hence only representing the mechanical factors *immediately* after surgery, where the implant was placed (without pretension). The biological growth was also not included in that analysis. This SCFE long-term growth analysis contains all three factors, as explained in section 2.2.6 and depicted in Figure 15. The sensitivity study in section 3.2.2 was performed to find the right thermal expansion coefficient α value to simulate one month of biological growth using thermal expansion and the right a and b values to simulate a month of mechanical growth. This chapter contains the results of the FE analysis of the SCFE *long-term* growth. The chapter is subdivided into three subsections: the first subsection contains the results of the biological growth for all screw positions and a visualisation of the stresses arising due to biological growth around the screw, the second subsection contains the results of the growth from all mechanical factors combined (the external load and the load due to bone-implant interaction) and the last subsection shows the results of the combined biological and mechanical growth, giving a complete view of the growth magnitude and pattern for the different screw positions. The rough outer ring of the growth plate is included in the visualisations to show the real position of the screw in the growth plate, but the results shown on the ring elements are not discussed and are excluded when calculating amounts of growth in the growth plate.

Biological growth

The results of the sensitivity analysis are used to simulate one month of growth as a result of biological factors. The external mechanical load is included in this analysis since this load influences the amount of biological growth, especially in SCFE patients, since SCFE is strongly associated with obesity [55, 56]. In Table 4 an overview is given of the average amount of growth in the growth plate due to biological factors for all screw positions. Figure 31 shows the expected amount of growth in the different areas of the growth plate (in mm/month).
It can be observed that biological growth always takes place, but is reduced by the presence of a screw. Figure 31a represents the case without a screw. It is interesting to see that the growth is also reduced in this configuration, because of the external load. The average biological growth in the growth plate without externally applied load was 0.4444 mm/month, as found in the sensitivity study. With the addition of the externally applied load it is reduced to 0.1862 mm/month, as can be seen in Table 4. In the screw cases, the biological growth is reduced in the vicinity of the screw. Directly around the screw, the growth is close to zero, but the further away from the screw, the closer the biological growth rate comes to the expected 0.5 mm/month and the more it resembles the values observed in the configuration without a screw. With the screw placed in the middle (Figure 31j), the screw reduces biological bone growth in a large area of the growth plate. The medial, anteromedial and posteromedial screw positions lead to the largest amount of biological growth, which appears mostly on the lateral side of the growth plate.
For the desire of bone growth on the posterior side in the case of slipped capital femoral epiphysis, the anterior, anterolateral and anteromedial screw position show most promising results in terms of biological bone growth by arresting growth on the anterior side whilst allowing growth on the posterior side.

Screw position	**Average biological growth in the growth plate (mm/month)**
No screw	0.1862
Anterior (A)	0.1623
Posterior (P)	0.1745
Medial (M)	0.1916
Lateral (L)	0.1109
Anteromedial (AM)	0.2136
Anterolateral (AL)	0.1705
Posteromedial (PM)	0.2513
Posterolateral (PM)	0.1665
Middle	0.0924

Table 4: The average amount of growth in the growth plate due to biological factors for the different screw positions (in mm/month).



(a) No screw (b) Anterior screw (c) Posterior screw

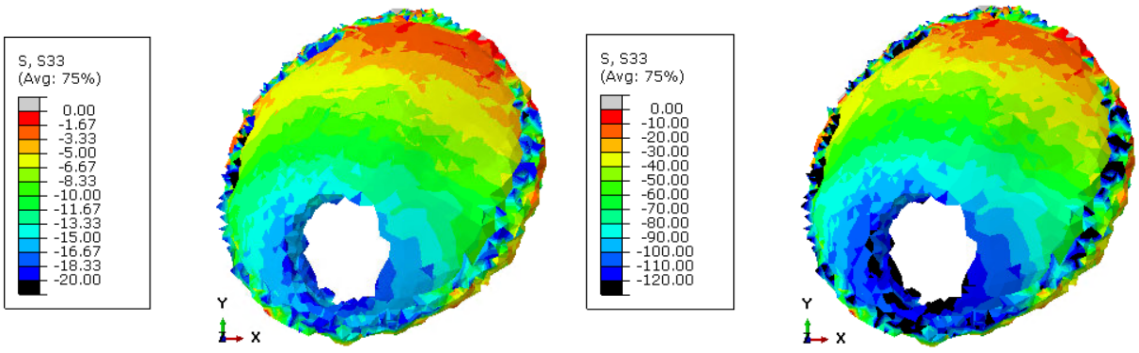
(d) Medial (e) Lateral (f) Anteromedial (g) Anterolateral

(h) Posteromedial (i) Posterolateral (j) Middle

Figure 31: The amount of biological growth in the growth plate for the different screw positions. The screw elements are removed for visualisation purposes.

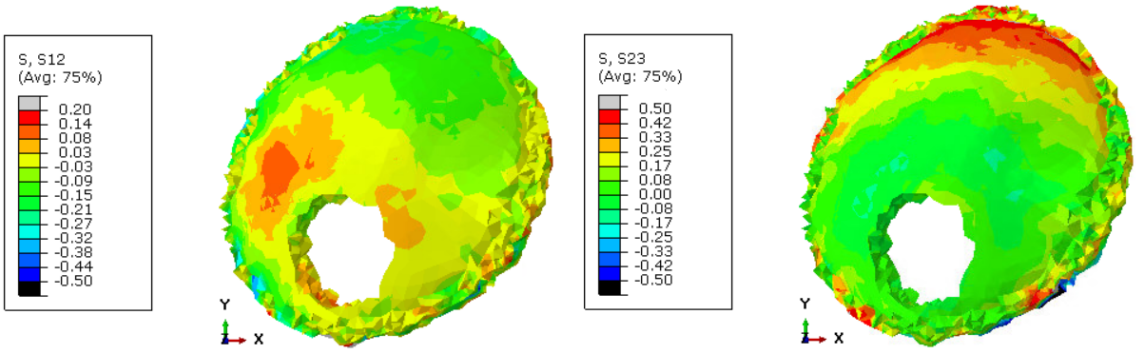
Stresses as a result of biological growth

Next to adding to the overall growth in the growth plate, the biological growth also introduces stresses around the screw which in turn influence the mechanical growth factors. In this subsection the stresses due to the bone-implant interaction are visualised. As an example a simulation with only biological growth (thermal expansion) and no external loads was performed on the anterior screw configuration. The results of this simulation can be seen in Figures 32 and 33 below. Figures 32a and 32b show the compressive stresses arising around the screw after one month and six months of growth, respectively. It can be observed that the pattern of compressive stresses is similar in both cases, but the magnitude of the compressive stresses increases with time. The highest compressive stress values are found closest to the screw, and the lowest values on the contralateral side. A study by [53] found a similar stress pattern and build-up of compressive stresses over time between the two staple legs of a Blount staple in a 2D model of the distal femur in an epiphyseal stapling case, although the magnitude of those stresses was slightly lower than the values found in this study. The compressive stress between the staple legs reached approximately -15 MPa after fifty days and -30 MPa after one hundred days.
Figure 33 shows the shear stresses in xy- and yz-direction after one month of growth. After one month, shear stresses in the xy-plane arise in the vicinity of the screw and shear stresses in the yz-plane arise on the contralateral side. The stresses introduced by the biological growth around the screw influence the growth in the growth plate. The compressive stresses influence the hydrostatic stress, leading to lower OI values in the areas of high compression and the shear stresses influence the octahedral shear stress, leading to higher OI values in the areas where the shear stresses are higher.



(a) (b)

Figure 32: The compressive stresses arising due to bone-implant interaction after a) one month and b) six months of biological growth.

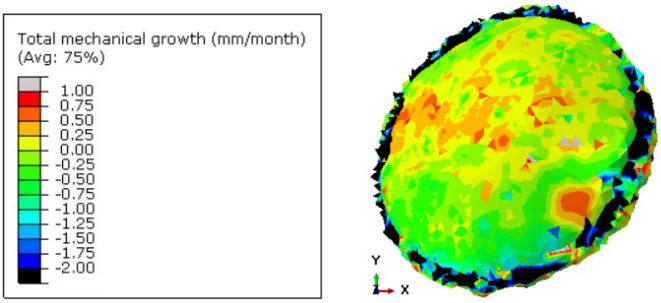


(a) (b)

Figure 33: The shear stresses arising due to bone-implant interaction after one month of biological growth in a) xy-direction and b) yz-direction.

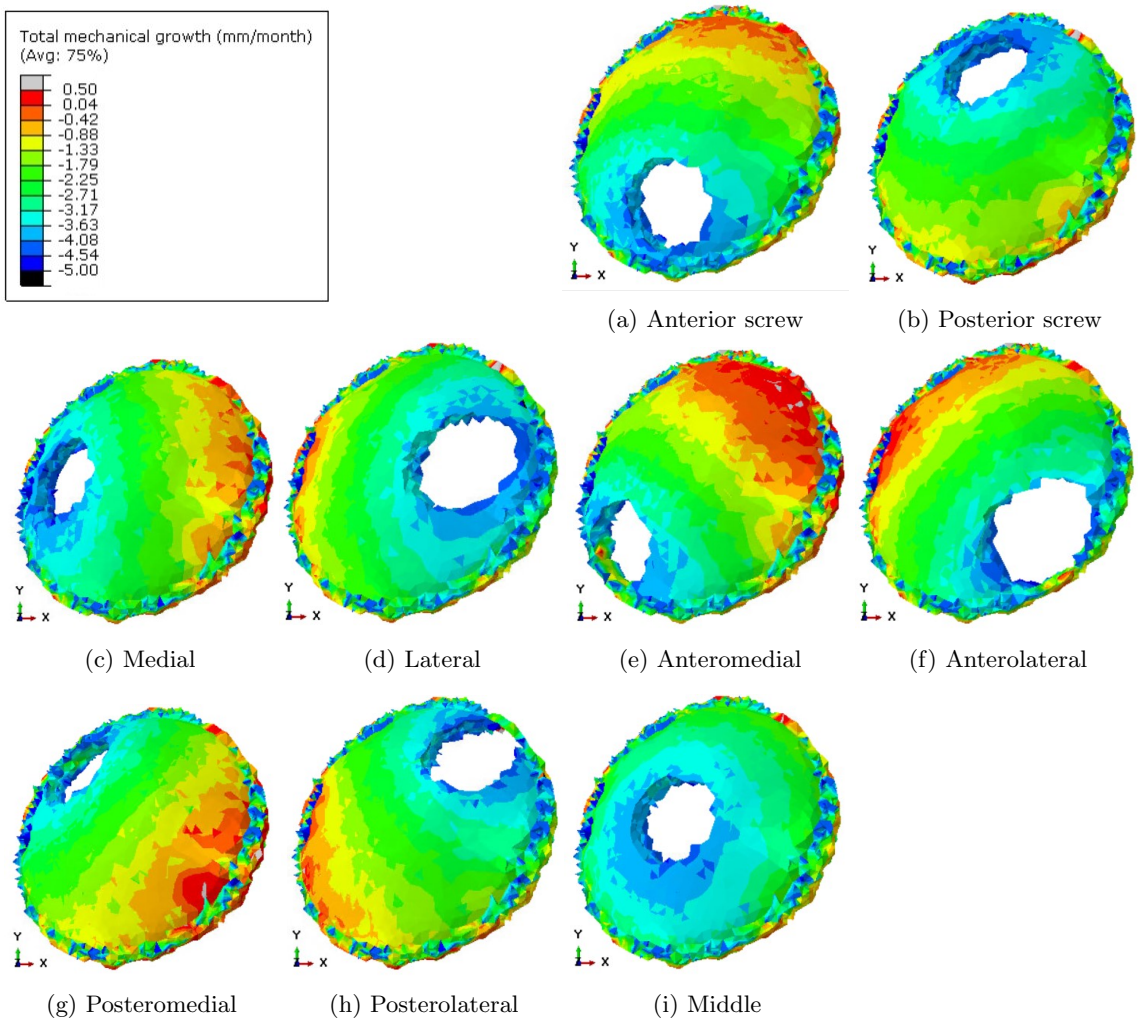
Total mechanical growth

Combining the stresses induced by the external load on the femur with the stresses induced by the bone-implant interaction, leads to all mechanical factors acting on the growth plate and hence the total expected amount of growth as a result of mechanical factors. The results of the FE analysis containing all these mechanical factors combined can be seen in a qualitative way in the form of the growth pattern in the growth plate (in mm/month) in Figures 34 and 35 below. Furthermore, a quantitative result of the amount of growth as a result of all mechanical factors is given in Table 5. The results indicate that the placement of a screw massively reduces the amount of growth as a result of mechanical factors. This is mainly due to the introduction of compressive stresses from the bone-implant interaction. Comparing these long-term total mechanical growth results to the instant mechanical growth results, it can furthermore be concluded that the effect of the external loads on mechanical growth (introducing octahedral shear stress on the opposite side of the growth plate from the screw) is far smaller than the effect of bone-implant interaction.
The highest amount of mechanical growth takes place when the screw is placed in anteromedial or anterolateral position. With the screw further away from the center, there is a smaller area influenced by the bone-implant interaction, as was seen in Figure 31. This leads to a smaller area with compressive stresses. The anteromedial and anterolateral screw positions allow for slightly more growth than the posteromedial and posterolateral screw positions, because these latter positions allow room for growth on the anterior half of the growth plate, but this is close to where the external load is applied, preventing large mechanical growth values.
As can be seen in Table 5, the total mechanical growth in the growth plate for the configuration without a screw is 0.2764 mm/month. In the same configuration without the thermal expansion for biological growth this was 0.2309 mm/month as found in the sensitivity study for mechanical growth. These values should have been equal, because the isolated effect of thermal expansion of the growth plate elements should not introduce stresses in the absence of a screw. This is further discussed in the Discussion.



(a) No screw

Figure 34: The total mechanical growth in the case with no screw.



(a) Anterior screw (b) Posterior screw

(c) Medial (d) Lateral (e) Anteromedial (f) Anterolateral

(g) Posteromedial (h) Posterolateral (i) Middle

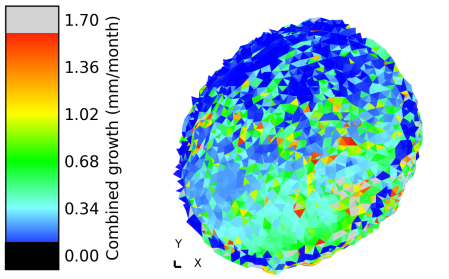
Figure 35: The total mechanical growth in the growth plate. This includes the mechanical growth as a result of the externally applied force and the bone-implant interaction. The screw elements are removed for visualisation purposes.

Screw position	**Total mechanical growth in the growth plate (mm/month)**
No screw	0.2764
Anterior (A)	0.0335
Posterior (P)	0.0088
Medial (M)	0.0250
Lateral (L)	0.0207
Anteromedial (AM)	0.0889
Anterolateral (AL)	0.0603
Posteromedial (PM)	0.0337
Posterolateral (PM)	0.0293
Middle	0.0048

Table 5: The average amount of growth in the growth plate due to the total mechanical factors (IIa and IIb) (in mm/month).

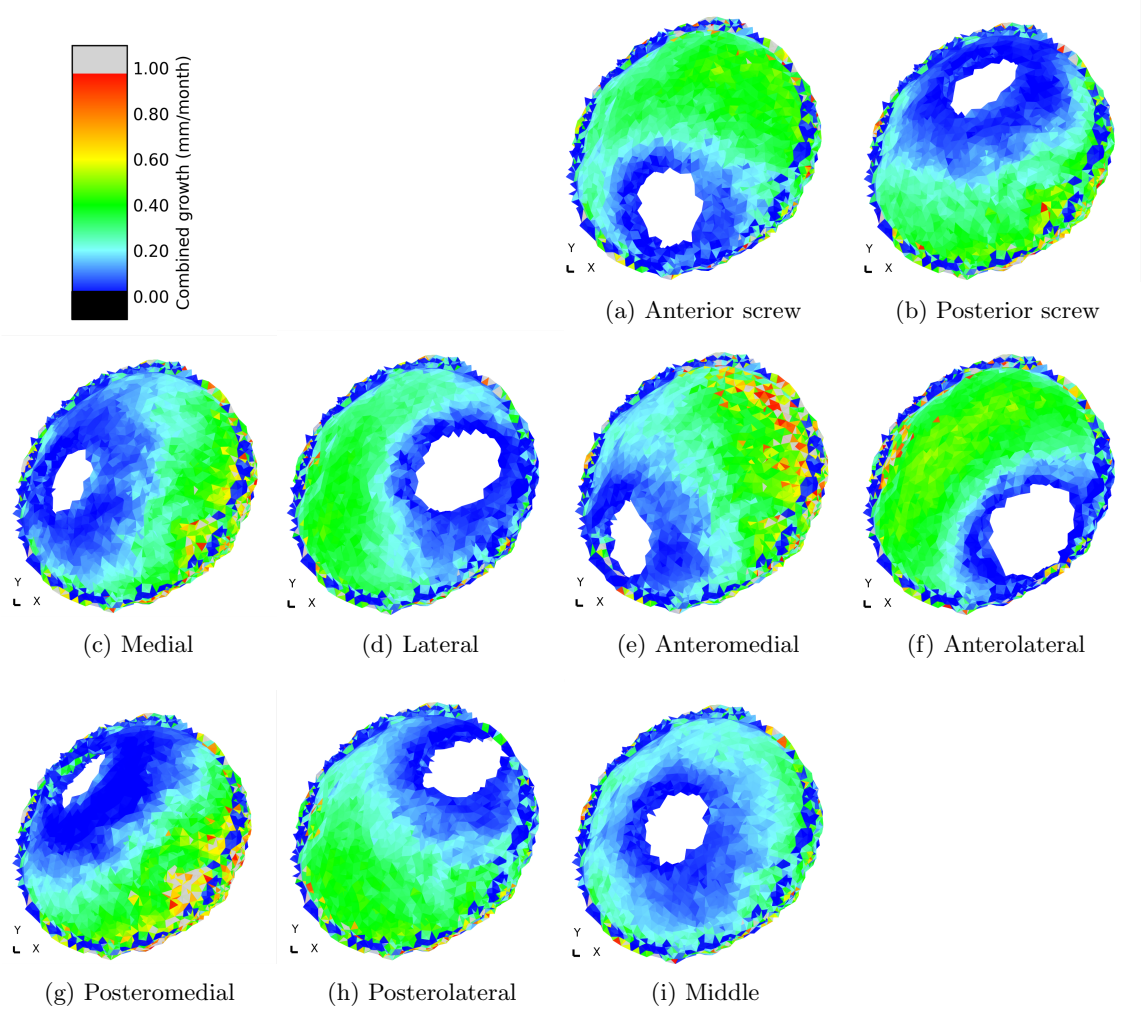
Combined growth

The results of the combined growth analysis for all configurations, using formula 10, can be seen in Figures 36 and 37 below. The finite element solutions were obtained from ABAQUS and post-processing was performed in Python. Figure 38 presents the total amount of growth in the growth plate for all ten configurations and the contribution of biological and mechanical factors to the total amount of growth. It can be observed that the configuration without a screw leads to the largest amount of growth, mostly due to a larger contribution of mechanical factors. The results also show that the screw in the middle (representing the center-center position currently used by surgeons) leads to the least amount of both biological and mechanical growth. Figures 36 and 37 illustrate the growth pattern for the different screw positions. With the screw positioned more to the exterior edges of the growth plate, more space remains for biological growth and the formation of octahedral shear stresses and hence mechanical growth, as can be most clearly seen in the anteromedial and posteromedial screw positions. Combining the results of the magnitudes of growth with the observed growth patterns, the best screw positions to stimulate growth on the posterior side of the growth plate are the anterior, anteromedial and anterolateral screw positions, with the anterior screw position leading to slightly less growth than the other two screw positions, but most clearly leading to growth on the posterior side.



(a) No screw

Figure 36: The combined growth in the case with no screw.



(a) Anterior screw (b) Posterior screw

(c) Medial (d) Lateral (e) Anteromedial (f) Anterolateral

(g) Posteromedial (h) Posterolateral (i) Middle

Figure 37: The combined growth in the growth plate. This includes the total mechanical growth and the biological growth. The screw elements are removed for visualisation purposes.

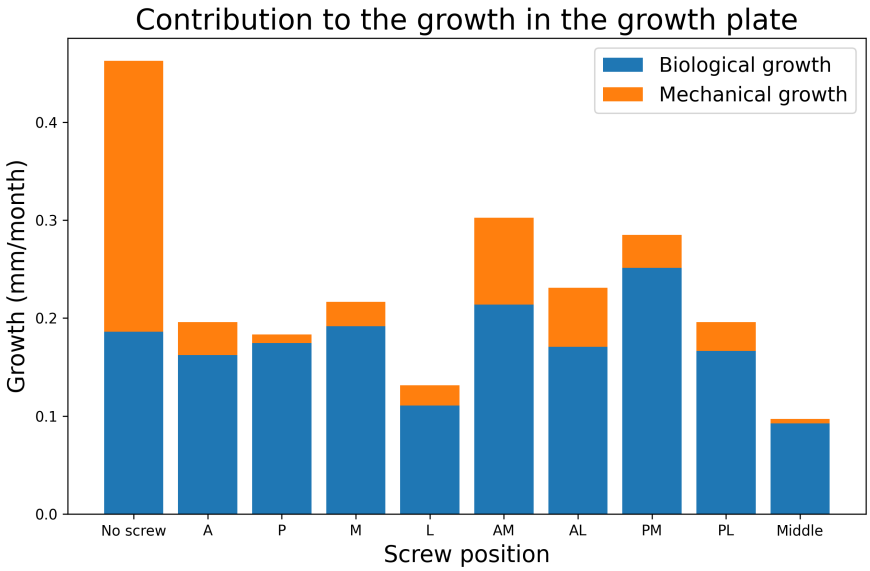


Figure 38: The contribution of the biological factors and the total mechanical factors to bone growth in the growth plate for the case without a screw and for all nine screw positions.

Comparison to Slobbe et al. [2]

A retrospective study by Slobbe et al. (2024) investigated the amount of proximal femoral growth after in-situ screw fixation of SCFE and the influence of the screw position on the amount of growth [2]. This is the first study analysing this correlation. 96 hips were included and the growth in the femur was examined measuring the Southwick angle, alpha angle and the displacement from Klein's line directly after surgery and at the final follow-up. The screw position was measured on anteroposterior and Lauenstein views. The results showed improvements in the Southwick angle at follow-up, supporting the hypothesis that growth continues after in-situ fixation, allowing for improvement in the femur morphology after surgery. The results of the multiple regression analysis indicated that a more anterior screw position is correlated with more improvement in the Southwick angle. For each percentage point that the screw was positioned more anteriorly, the Southwick angle improved by 0.33° [2].
The results obtained in this study mostly align with those results. In this study anterior, anteromedial and anterolateral screw positions were the only configurations leading to high combined growth values on the posterior side of the physis. This indicates growth on the posterior side of the physis, which is expected to tilt the femoral head anteriorly, thereby decreasing the Southwick angle. The posteromedial, posterolateral and posterior screw positions stimulated growth on the anterior side of the growth plate, stimulating the opposite effect.

4 Discussion

This study aimed to investigate the optimal screw position for in-situ fixation in slipped capital femoral epiphysis (SCFE) using finite element analysis. This chapter critically reflects on the results, discusses the limitations and the considerations that need to be acknowledged when interpreting the findings and provides recommendations for future research before ending with the conclusion.

4.1 Healthy growth analysis

The overall growth pattern resulting from the healthy growth analysis showed good resemblance with the growth pattern found in the study by [1]. The largest differences in the growth pattern were observed in the femoral neck, with higher stresses in that region in the results of this study compared to the study by [1]. This can be explained by the differences in geometry, with the femur in this study having a longer and smaller neck than the femur in the study by [1]. A smaller cross-sectional area to carry the external load leads to higher stress values in that area. In both studies the highest OI values were observed right above the growth plate with additional elevated OI values in the femoral neck. Although the growth pattern showed good resemblance, the OI values observed in this study were slightly higher than the ones observed in the study by [1]. An explanation for this could be the difference in load magnitude applied on the femur, which was higher in this study due to the higher weight of the patient used in this study. Other explanations could be the differences in femur shape and growth plate position and shape, as these were found to highly influence the stress distribution [1]. The growth pattern observed in this study could not explain the decrease in neck-shaft angle observed on the CT scans of the patient. This discrepancy could be due to the exclusion of biological growth in this analysis. Given that high mechanical loads are known to suppress biological growth, and that the external mechanical load in this study is applied with a slight medial inclination (15° in the coronal plane), it is likely that the biological growth rate would have been higher on the lateral side if considered, which would have led to a decrease in NSA.

4.2 ABAQUS vs MIMICS growth plate generation

In this study two different methods for generating the growth plate were compared: 1) creating the growth plate in ABAQUS by assigning the right material properties to the elements in the growth plate region and 2) creating the growth plate in MIMICS by creating a mask on the CT scan. This comparison was also performed by [1] before and the findings were similar. The ABAQUS is much simpler to implement, but the MIMICS method leads to a much smoother growth plate surface, because the growth plate is taken into account when creating the mesh. The difficulty arising from the MIMICS method is that the software makes some adjustments when converting a mask to a part. In this case this led to many overlapping triangles between the growth plate surface and the femur surface, such that no good mesh could be created in 3-Matic where the growth plate fitted nicely in the femur. As a result, the growth plate had to be segmented such that it fell completely within the femur model, using Boolean operations. The elements on the edges of the growth plate had to be added to the growth plate region in ABAQUS later on. This led to rough edges, but with the ABAQUS method the entire growth plate surface is rough. Despite the added complexity of the MIMICS method, this method was preferred over the ABAQUS method because of the smoother result. Especially with the use of thermal expansion, a smooth surface was desired to avoid stresses as a result of element-interaction where growth plate elements are not free to expand. Furthermore,

it should be taken into account that the material assignment methods by both the *by mask* option in MIMICS and the *getbyboundingsphere* function in ABAQUS only select the elements that fall *completely* within the mask or sphere. Elements that belong to the growth plate but fall slightly out of the mask or sphere because of the meshing in 3-Matic are not assigned the growth plate material. This can be clearly seen in the FE growth plate model created by ABAQUS in the study by [1] which is thinner than the intended 3 mm. In this study those elements are manually added to the growth plate region in ABAQUS to assure a complete and smooth growth plate with the right material properties. This is visualised in Appendix E.

4.3 SCFE Instant growth

The instant growth due to mechanical factors was found to be highest on the posterior side of the growth plate. This can be explained by the external load being applied on the anterior side. This finding is in line with the results of a study by Piszczatowski et al. [57] who found that the lowest OI values are in the region to which the applied load is directed and the maximum OI appears in regions where the growth plate surface is almost parallel to the loading direction. The growth plate in the SCFE femur model is indeed almost parallel to the external load on the posterior side, where the OI values are highest. The study by Piszczatowski also observed that the growth pattern is non-uniform in the growth plate when it is located between two bone blocks. This is also observed in this study.

In the anterior and anterolateral configurations of the screw, the compressive stresses right after surgery were close to zero. This could be explained by the screw carrying the compressive stresses rather than the growth plate, as was also found in a study by [50]. It was observed that when the screw carries all the external load, the growth magnitude due to mechanical factors is largely reduced. In the other configurations, however, the compressive stresses were much higher than in the case without a screw. A possible explanation for this is that the compressive forces are not spread over the growth plate like in the cases without a screw because of the presence of the screw, leading to higher compressive stresses. In some of the configurations these high compressive stresses were accompanied by octahedral shear stresses on the contralateral side, promoting bone growth, with only the medial, anteromedial and posteromedial screw positions leading to instant mechanical growth on the desired posterior side of the growth plate. Future research could further look into these capabilities of screws to both reduce the initial compressive stresses by carrying the load and increase the compressive stresses when the screw is not in the vicinity of the externally applied load.

4.4 SCFE long-term growth

The SCFE long-term growth analysis was split up in different parts. The analysis only including the biological growth for the different screw positions revealed that biological growth still takes place with, but is reduced by, the presence of the screw. It is mostly reduced in the vicinity of the screw, but shows increasing values as the distance from the screw increases. The middle screw position showed the lowest magnitude of biological growth, as it inhibited growth in a large area. The anterior, anteromedial and anterolateral positions showed most promising results with high growth values (up until 0.21 mm/month compared to 0.19 mm/month in the configuration without a screw) and growth on the posterior side of the growth plate.

The results of the analysis with all mechanical factors included showed a large decrease in growth with the presence of a screw. The addition of the bone-implant interaction forces induced high compressive stresses around the screw, inhibiting mechanical bone growth. The anteromedial and anterolateral were the only two configurations with noteworthy mechanical growth on the posterior side. Those screw positions were on the edges of the growth plate half where the load is applied, leaving room for growth-stimulating octahedral shear stresses to arise on the contralateral side.
The results of the combined growth analysis showed that the amount of growth is reduced by roughly 50% with the presence of a screw. This is mostly resulting from a decrease in mechanical growth. The middle screw position showed the smallest amount of growth in both the biological and mechanical growth. The anteromedial, anterolateral and posteromedial positions showed the largest amount of growth, with the anteromedial and anterolateral showing growth on the desired posterial side of the growth plate. The anterior screw showed a slightly lower amount of growth, but showed the most beneficial growth pattern. This mostly resembles the results of the biological growth analysis, as this factor had the largest contribution to combined growth. The analyses revealed that the biological growth results of the posterior, medial and posterolateral positions of the screw were amongst the highest values, but the mechanical growth values for these positions were low, such that the combined growth magnitude was not as high as in other configurations.

4.5 Comparison to Slobbe et al. [2]

The methodology employed in this study has some noticeable differences with the methodology used in the retrospective study by [2]. These differences pose challenges for direct comparison. The study by Slobbe et al. measured screw positions on anteroposterior (AP) and Lauenstein views, focusing solely on the relative anterior versus posterior and medial versus lateral positions without accounting for potential combinations of these positions. Their results correlated screw positions on the AP line with improvements in Southwick angle, but this does not say anything about the extent to which a screw is placed medially or laterally. This study, on the contrary, also included combined positions such as the anteromedial and the posterolateral position. It is likely that these positions would have been categorised under an 'anterior' and 'posterior' placement in Slobbe et al.'s methodology, respectively, but this cannot be guaranteed. The most significant challenge in comparing the results lies in the presentation of the results. Slobbe et al. measured changes in Southwick angle on Lauenstein views, while this study presented results through the growth patterns on the growth plate. The absence of growth visualisation in the form of updated 3D geometry and the lack of orientation of the femur model within the patient's overall anatomy hinder the ability to quantify the expected growth in terms of changes in Southwick angle. The results of both studies can hence be compared to some extent, but the differing natures of the methodologies should be considered when doing so.

4.6 FE model generation

In this study, the growth plate was taken as a sphere and oriented with the use of the CT scan images. The growth plate thickness was assumed to have a thickness of 3 mm. Although the location and orientation of the growth plate in the model are assumed to be quite accurate because of the use of the medical images, the real shape of a growth plate is not a perfect sphere. The shape was hence simplified. In addition, in reality the growth plate thickness varies throughout the growth plate and also varies over time. As a study by Yadav et al. [21] found that the growth plate

shape has an effect on the osteogenic index, this simplification might have influenced the results of this study. Additionally, the secondary center of ossification was not included in this study. The exclusion of this anatomical feature might impact the accuracy of the bone growth simulation, as it plays a role in the overall growth process of the femur. Future studies should consider incorporating this factor to enhance the model's realism.

It was decided to mesh the model in Materialise rather than in ABAQUS, because Materialise allows the assignment of real density and elasticity values to every element with the use of grey scale values, providing a more accurate representation than meshing directly in ABAQUS and assigning general material properties that do not match the patient's specific tissue properties. However, the meshing limitations imposed by Materialise also introduce certain constraints. Materialise only allows the creation of a tetrahedral mesh, which becomes fixed when imported into ABAQUS. This rigidity complicates the creation of an iterative process using thermal expansion in the growth plate. The element shape for instance prevented the possibility to grow elements isotropically and easily split elements in half when a certain volume is reached, as done in [47], to update the mesh and create an iterative growth algorithm.

The tetrahedral mesh furthermore presents another limitation. The biological growth alone should not introduce stresses in the case without a screw. However, the current model shows some small stresses arising from the thermal expansion in the case without a screw. This is likely due to the tetrahedral elements not being completely free to move in the direction of thermal expansion, possibly because of the geometric constraints inherent in their shape. Tetrahedral elements, especially when densely packed, can experience more inter-element interaction compared to structured meshes like hexahedral or layered quadratic elements, which align more naturally with mechanical deformations. This could be resolved using quadratic elements in the growth plate that are perfectly layered, along with a local material orientation in the growth plate elements. Such modifications would ensure that the elements have more uniform deformation characteristics, minimising the unintended stresses.

The result plots created with ABAQUS showed differences in visual presentation with the plots created in Python by the author of this study for the combined growth using the FE analysis results exported from ABAQUS. The biological growth and total mechanical growth for the case with no screw (in this study plotted in ABAQUS directly) were also plotted with the Python script used for the combined growth visualisation to show the visual differences between both methods. This can be observed in Appendix H. Specifically, the ABAQUS plots present a smooth appearance, whereas in some of the Python-generated plots the elements of the tetrahedral mesh can be observed. This discrepancy can be attributed to the interpolation techniques employed by ABAQUS. ABAQUS utilises interpolation methods to estimate and smooth the values between mesh elements to make the plots more continuous and visually appealing. In contrast, the Python plots display the raw, unprocessed data, directly reflecting the discrete values within each tetrahedral element without any form of interpolation. This direct representation highlights the individual mesh elements, making the triangular structure of the mesh visible in some of the plots. Understanding this difference is crucial for interpreting the figures accurately.

4.7 Growth Analysis

A significant limitation arises from the uncertainty regarding the loading direction of the hip-reaction forces on the femur in slipped capital femoral epiphysis. The direction of these forces can vary significantly between patients and is challenging to determine without detailed musculoskeletal modeling. In literature, a wide variety of applied load directions on the femur is used, often directed towards the center of the femoral head at certain angles. However, for SCFE, the specific angles of these forces are even less understood. In this study, the load magnitude was estimated based on body weight and the direction of the normal hip contact force found in literature and the assumption that the loading remains in the same position relative to the femoral neck. This estimation forms a limitation as the loading condition influences the stresses and strains in the bone and cartilage, eventually affecting the growth pattern, and there is insufficient evidence that this loading location and direction is accurate.

In this study only the hip contact forces are modelled. This is done in many other studies [54]. It is believed that omitting the muscle forces does not have a great influence on the results, because a previous study by [24] found that muscles have little effect on the stresses in the growth plate. In SCFE patients, with high hip contact forces due to high body weight, this effect is assumed to be even smaller. Moreover, similar to multiple other studies [32, 47, 58, 59], this study did not differentiate between static and cyclic loading. This might have influenced the results, as static stress is believed to reduce the growth rate, whereas cyclic changes of dynamic loading and unloading is believed to increase the growth rate according to the Hueter-Volkman law [60, 61, 50].

Although this study incorporates a bone-implant interaction study to model the stresses around the screw, a more thorough investigation into this topic is required to fully understand the underlying mechanisms. This study simulated one month of biological growth and examined the resultant stresses arising around the screw. It is not yet fully understood to what extent the cartilage in the growth plate continues to grow around the screw and at what point this concludes and the growth plate closes prematurely in this area and what effect this has on the stresses around the screw.

Finally, the thermal expansion in the model was simulated as orthogonal in the global z-direction. While this method provides a simplified approach, the direction of thermal expansion does influence the growth pattern. To gain a more accurate understanding of the growth pattern in SCFE patients, growth direction models such as growth in the femoral neck deflection direction and growth in the maximal principal stress directions should be incorporated in the model and calculated for each element individually. Studies by [62] and [63] showed observational evidence of both these models.

The results of the combined growth show that the proportion of biological and total mechanical growth is not equal to two-thirds and one-third as often used in literature (this can be seen in Figure 38). In many computational studies, the contribution of biological factors to bone growth is assumed to be approximately two-thirds of the total growth, with mechanical factors accounting for the remaining one-third. This assumption is based on findings of one study by Hall et al. from 1990 [45]. This study performed avian embryo paralysis experiments, which showed that in the absence of mechanical loading, femoral growth reached 63% of its normal rate. However, this fixed ratio may oversimplify the complex interplay between biological and mechanical factors. In reality, these factors are likely interdependent; biological growth can alter the stress pattern in the growth plate and mechanical loads can influence biological processes, potentially altering growth rates and the

ratio of contribution to growth of both factors. For instance, high mechanical loading suppresses biological growth rates, which is the principle underlying the use of knee staples. Therefore, while the total growth rate might remain consistent, the relative contributions of biological and mechanical factors may shift depending on the specific mechanical environment. In this context, the two-thirds to one-third ratio observed in an isolated scenario (like a paralysed state) may not directly translate to normal physiological conditions, where both mechanical and biological stimuli are present. The results of the present study, which deviated from this often used ratio, may reflect this more dynamic interaction, where the mechanical environment influenced the biological response, leading to a different growth contribution ratio. Further research is necessary to investigate how mechanical and biological factors influence each other during bone growth and how their contributions may vary across different loading conditions.
In addition, the bone growth contribution ratio might be different due to the altered anatomy of the femur. This abnormal morphology of the femur might influence the mechanical environment and thereby also the mechanical contribution to bone growth. A slipped femoral head changes the orientation of the external load compared to the femoral head and growth plate and thereby likely introduces higher shear stresses in the growth plate, particularly in the configuration without a screw. This could explain why the mechanical contribution to growth in the case without a screw is larger than the biological contribution.

4.8 Recommendations for future work

For more accurate modelling of the growth pattern in SCFE patients, future research should focus on obtaining the loads in these patients from musculoskeletal models using inverse dynamics in gait. This would allow to include multiple load cases rather than the single load case used in this study, to gain a better understanding of the stresses throughout the gait cycle. An even more useful addition would be dynamic loading of the model, as cyclic changes of dynamic loading and unloading were found to increase the growth rate [60, 61, 50]. Focus should furthermore be on investigating the differences in loading between different individuals and different severity's of the slip.

As a next step, the model could be expanded by making it an iterative process. Elements in the growth plate could be expanded using thermal expansion and nodal coordinates could be updated. Elements could be split once a certain volume is reached, after which the material properties in the exterior element layer could be altered to simulate ossification. This would allow to model the growth in the femur for a longer period of time, hence giving a more complete view of the growth pattern under different screw positions. It would also visualise the growth in 3D, such that more accurate statements can be made regarding the changes in important SCFE characteristics such as the Southwick angle, alpha angle and displacement from Klein's line. This would allow for easier comparison with clinical observations and validation of the growth modelling of the SCFE femur after in-situ fixation as suggested in this study.

Another interesting area of research would be to investigate the influence of slip severity on the growth pattern under a certain screw position. This study modelled growth for one patient with a moderate slip, but it is still unknown whether the same recommendations would hold for a less or more severe slip of the femoral head.

4.9 Conclusion

This study aimed to answer the following question: *What is the optimal screw position for in-situ fixation of slipped capital femoral epiphysis to stimulate longitudinal bone growth on the posterior side of the growth plate?* The results showed that the middle screw position - which represents the position currently used by surgeons - leads to low growth values in the growth plate. This position showed the lowest magnitude of both biological and mechanical growth of all nine modelled screw positions, mostly due to the limited amount of space for biological growth in the growth plate. The highest amount of combined growth was found for the anteromedial, anterolateral and posteromedial screw positions with the anteromedial and anterolateral screw positions showing the most beneficial growth pattern with observed growth on the posterolateral and posteromedial side of the growth plate, respectively. The anterior screw position showed a slightly smaller amount of combined growth, but showed the most beneficial growth pattern with growth on the posterior side of the growth plate. These findings support the hypothesis and the findings of the study by [2] that an anteriorly placed screw might positively influence bone growth in SCFE patients.

In conclusion, this study marks an initial step towards reconsidering the conventional center-center screw position in the treatment of slipped capital femoral epiphysis. The findings suggest that an anterior screw position could positively influence bone growth after in-situ fixation by promoting growth on the posterior side of the growth plate. The results show potential for the use of anteriorly placed screws in guided bone growth to mitigate slip severity and enhance femoral anatomy restoration. Implementing these insights in practice could pave the way for improved surgical strategies aimed at achieving better long-term functional and structural outcomes for SCFE patients. Further research and clinical validation are required to explore the full implications and practical application of these findings in optimising treatment strategies for SCFE patients.

References

[1] P. Roels, R. Agricola, E. Oei, H. Weinans, G. Campoli, and A. Zadpoor, "Mechanical factors explain development of cam-type deformity," *Osteoarthritis and Cartilage*, vol. 22, no. 12, pp. 2074–2082, 2014.

[2] J. Slobbe, C. L. P. Van de Ree, J. H. Bessems, and J. J. Tolk, "Remodeling after in situ pinning for Slipped Capital Femoral Epiphysis; The influence of transphyseal screw position.".

[3] C. L. Lehmann, R. R. Arons, R. T. Loder, and M. G. Vitale, "The epidemiology of slipped capital femoral epiphysis: An update," *Journal of Pediatric Orthopaedics*, vol. 26, no. 3, 2006.

[4] J. D. Chlebeck, C. E. Birch, and J. W. Lisle, "Percutaneous in situ fixation of slipped capital femoral epiphysis," *JBJS Essential Surgical Techniques*, vol. 6, no. 1, 2016.

[5] K. Peck and J. Herrera-Soto, "Slipped Capital Femoral Epiphysis: What's New?," *Orthopedic Clinics of North America*, vol. 45, pp. 77–86, 1 2014.

[6] R. T. Loder, "The demographics of slipped capital femoral epiphysis: An international multicenter study," in *Clinical Orthopaedics and Related Research*, vol. 322, 1996.

[7] G. Hagglund, L. I. Hansson, and G. Ordeberg, "Epidemiology of slipped capital femoral epiphysis in southern Sweden," *Clinical Orthopaedics and Related Research*, vol. NO. 191, 1984.

[8] S. Senthi, P. Blyth, R. Metcalfe, and N. S. Stott, "Screw placement after pinning of slipped capital femoral epiphysis: A postoperative CT scan study," *Journal of Pediatric Orthopaedics*, vol. 31, pp. 388–392, 6 2011.

[9] C. A. Makarewich, E. S. Md, G. T. Fedorak, and B. A. MacWilliams, "Factors Affecting Slip Progression After In Situ Screw Fixation of Stable Slipped Capital Femoral Epiphysis," *Journal of pediatric orthopedics*, vol. 42, pp. E414–E420, 5 2022.

[10] B. T. Carney, P. Birnbaum, and C. Minter, "Slip progression after in situ single screw fixation for stable slipped capital femoral epiphysis," *Journal of pediatric orthopedics*, vol. 23, pp. 584–589, 9 2003.

[11] B. Carney, S. Weinstein, and J. Noble, "Long-term follow-up of slipped capital femoral epiphysis. ," *J Bone Joint Surg Am.*, vol. 73, pp. 667–674, 6 1991.

[12] C. E. Jones, A. P. Cooper, J. Doucette, L. L. Buchan, D. R. Wilson, K. Mulpuri, and A. G. D'Entremont, "Relationships between Severity of Deformity and Impingement in Slipped Capital Femoral Epiphysis," *Journal of Pediatric Orthopaedics*, vol. 37, no. 4, pp. 272–278, 2017.

[13] B. T. Carney and S. L. Weinstein, "Natural history of untreated chronic slipped capital femoral epiphysis," in *Clinical Orthopaedics and Related Research*, vol. 322, 1996.

[14] G. E. M. Kennedy, J. Pullan, and A. El-Bakoury, "Comparing pinning in situ and capital realignment procedures for severe, stable slipped capital femoral epiphysis: a systematic review," *Journal of hip preservation surgery*, vol. 10, pp. 238–243, 12 2023.

[15] V. V. Upasani, T. H. Matheney, S. A. Spencer, Y. J. Kim, M. B. Millis, and J. R. Kasser, "Complications after modified Dunn osteotomy for the treatment of adolescent slipped capital femoral epiphysis," *Journal of pediatric orthopedics*, vol. 34, no. 7, pp. 661–667, 2014.

[16] J. Örtegren, L. Björklund-Sand, M. Engbom, and C. J. Tiderius, "Continued Growth of the Femoral Neck Leads to Improved Remodeling after in Situ Fixation of Slipped Capital Femoral Epiphysis," *Journal of Pediatric Orthopaedics*, vol. 38, no. 3, pp. 170–175, 2018.

[17] D. A. Kumm, S. H. Lee, M. H. Hackenbroch, and J. Rütt, "Slipped capital femoral epiphysis: A prospective study of dynamic screw fixation," *Clinical Orthopaedics and Related Research*, vol. 384, 2001.

[18] C. Öhman, M. Baleani, C. Pani, F. Taddei, M. Alberghini, M. Viceconti, and M. Manfrini, "Compressive behaviour of child and adult cortical bone," *Bone*, vol. 49, pp. 769–776, 10 2011.

[19] J. P. Berteau, M. Pithioux, C. Baron, E. Gineyts, H. Follet, P. Lasaygues, and P. Chabrand, "Characterisation of the difference in fracture mechanics between children and adult cortical bone," *Computer Methods in Biomechanics and Biomedical Engineering*, vol. 15 Suppl 1, pp. 281–282, 2012.

[20] J. Guevara, M. Moncayo, J. Vaca-González, M. Gutiérrez, L. Barrera, and D. Garzón-Alvarado, "Growth plate stress distribution implications during bone development: A simple framework computational approach," *Computer Methods and Programs in Biomedicine*, vol. 118, no. 1, pp. 59–68, 2015.

[21] P. Yadav, S. J. Shefelbine, and E. M. Gutierrez-Farewik, "Effect of growth plate geometry and growth direction on prediction of proximal femoral morphology," *Journal of Biomechanics*, vol. 49, pp. 1613–1619, 6 2016.

[22] G. Bergmann, G. Deuretzbacher, M. Heller, F. Graichen, A. Rohlmann, J. Strauss, and G. N. Duda, "Hip contact forces and gait patterns from routine activities," *Journal of Biomechanics*, vol. 34, pp. 859–871, 7 2001.

[23] A. Carriero, A. Zavatsky, J. Stebbins, T. Theologis, G. Lenaerts, I. Jonkers, and S. J. Shefelbine, "Influence of altered gait patterns on the hip joint contact forces," *Computer Methods in Biomechanics and Biomedical Engineering*, vol. 17, no. 4, 2014.

[24] A. Carriero, *Modelling gait abnormalities and bone deformities in children with CP.* PhD thesis, Imperial College London, 2009.

[25] M. Pines and S. Hurwitz, "The Role of the Growth Plate in Longitudinal Bone Growth," *Poultry Science*, vol. 70, pp. 1806–1814, 8 1991.

[26] D. Carter, T. Orr, D. Fyhrie, and D. Schurman, "Influences of mechanical stress on prenatal and postnatal skeletal development," *Clin Orthop Relat Res*, vol. 219, pp. 237–250, 1987.

[27] D. R. Carter and M. Wong, "Mechanical stresses and endochondral ossification in the chondroepiphysis," *Journal of Orthopaedic Research*, vol. 6, no. 1, 1988.

[28] M. Wong and D. R. Carter, "A theoretical model of endochondral ossification and bone architectural construction in long bone ontogeny," *Anatomy and embryology*, vol. 181, pp. 523–532, 7 1990.

[29] S. S. Stevens, G. S. Beaupre, and D. R. Carter, "Computer model of endochondral growth and ossification in long bones: Biological and mechanobiological influences," *Journal of Orthopaedic Research*, vol. 17, no. 5, pp. 646–653, 1999.

[30] S. Shefelbine, C. Tardieu, and D. Carter, "Development of the femoral bicondylar angle in hominid bipedalism," *Bone*, vol. 30, no. 5, pp. 765–770, 2002.

[31] S. Shefelbine and D. Carter, "Mechanobiological predictions of growth front morphology in developmental hip dysplasia," *Journal of Orthopaedic Research*, vol. 22, no. 2, pp. 346–352, 2004.

[32] A. Carriero, I. Jonkers, and S. Shefelbine, "Mechanobiological prediction of proximal femoral deformities in children with cerebral palsy," *Computer Methods in Biomechanics and Biomedical Engineering*, vol. 14, no. 3, pp. 253–262, 2011.

[33] N. Rutten, "Effect of different femur shapes on the development of cam-type deformities," tech. rep., Delft University of Technology, 2021.

[34] H. Kainz, B. A. Killen, M. Wesseling, F. Perez-Boerema, L. Pitto, J. M. G. Aznar, S. Shefelbine, and I. Jonkers, "A multi-scale modelling framework combining musculoskeletal rigid-body simulations with adaptive finite element analyses, to evaluate the impact of femoral geometry on hip joint contact forces and femoral bone growth," *PLoS ONE*, vol. 15, 7 2020.

[35] N. Ebert, M. Rupprecht, R. Stuecker, S. Breyer, N. Stiel, M. H. Priemel, and A. S. Spiro, "Outcome of the modified Dunn procedure in severe chronic or acute on chronic slipped capital femoral epiphysis," *Journal of Orthopaedic Surgery and Research*, vol. 14, pp. 1–7, 11 2019.

[36] S. Stacey, W. Barfield, L. Pietrykowski, J. DesJardins, and J. Mooney, "Comparison of Fatigue Performance Between Fully and Partially Threaded Cannulated Screws Used for Stabilization of Slipped Capital Femoral Epiphyses.," *Journal of surgical orthopaedic advances*, vol. 26, no. 1, 2017.

[37] A. Gefen, "Computational simulations of stress shielding and bone resorption around existing and computer-designed orthopaedic screws," *Medical and Biological Engineering and Computing*, vol. 40, no. 3, pp. 311–322, 2002.

[38] AZO Materials, "Titanium Alloys - Ti6Al7Nb Properties and Applications."

[39] J. A. Inzana, P. Varga, and M. Windolf, "Implicit modeling of screw threads for efficient finite element analysis of complex bone-implant systems," *Journal of Biomechanics*, vol. 49, pp. 1836–1844, 6 2016.

[40] Z. Fishkin, D. G. Armstrong, H. Shah, A. Patra, and W. M. Mihalko, "Proximal femoral physis shear in slipped capital femoral epiphysis - A finite element study," *Journal of Pediatric Orthopaedics*, vol. 26, pp. 291–294, 5 2006.

[41] J. W. Pritchett and K. D. Perdue, "Mechanical factors in slipped capital femoral epiphysis," *Journal of pediatric orthopedics*, vol. 8, no. 4, pp. 385–388, 1988.

[42] H. D. Aitken, Y. M. Yen, A. M. Kiapour, W. M. Sailer, J. B. Holt, J. E. Goetz, and E. J. Scott, "The Effects of Residual Femoral Deformity on Computed Contact Mechanics in Patients Treated with in Situ Fixation for Slipped Capital Femoral Epiphysis," *Journal of Pediatric Orthopaedics*, vol. 44, pp. E218–E225, 3 2024.

[43] K. Johns, A. Mabrouk, and M. M. Tavarez, "Slipped Capital Femoral Epiphysis," *StatPearls*, 7 2023.

[44] J. W. Pritchett, "Longitudinal growth and growth-plate activity in the lower extremity," *Clinical Orthopaedics and Related Research*, vol. 275, pp. 274–279, 1992.

[45] B. K. Hall and S. W. Herring, "Paralysis and growth of the musculoskeletal system in the embryonic chick," *Journal of morphology*, vol. 206, no. 1, pp. 45–56, 1990.

[46] J. A. Germiller and S. A. Goldstein, "Structure and function of embryonic growth plate in the absence of functioning skeletal muscle," *Journal of orthopaedic research : official publication of the Orthopaedic Research Society*, vol. 15, no. 3, pp. 362–370, 1997.

[47] S. Sadeghian, F. Shapiro, and S. Shefelbine, "Computational model of endochondral ossification: Simulating growth of a long bone.," *Bone*, vol. 153, p. 116132, 12 2021.

[48] C. K. Boese, J. Dargel, J. Oppermann, P. Eysel, M. J. Scheyerer, J. Bredow, and P. Lechler, "The femoral neck-shaft angle on plain radiographs: a systematic review," *Skeletal Radiology*, vol. 45, pp. 19–28, 1 2016.

[49] T. Schlégl, V. Nyakas, D. Kovács, P. Maróti, G. Józsa, and P. Than, "Neck-shaft angle measurement in children: accuracy of the conventional radiography-based (2D) methods compared to 3D reconstructions," *Scientific Reports*, vol. 12, no. 1, 2022.

[50] L. Hucke, J. Holder, S. van Drongelen, F. Stief, A. Gámez, A. Huß, and A. Wittek, "Influence of tension-band plates on the mechanical loading of the femoral growth plate during guided growth due to coronal plane deformities," *Frontiers in Bioengineering and Biotechnology*, vol. 11, 2023.

[51] M. Schneider, J. Buschbaum, A. Joeris, O. Röhrle, J. Dwyer, J. B. Hunter, R. A. Reynolds, T. F. Slongo, B. Gueorguiev, and P. Varga, "Biomechanical investigation of two long bone growth modulation techniques by finite element simulations," *Journal of Orthopaedic Research*, vol. 36, pp. 1398–1405, 5 2018.

[52] D. I. Bylski-Austrow, E. J. Wall, M. P. E. Rupert, D. R. Roy, and A. H. Crawford, "Growth Plate Forces in the Adolescent Human Knee: A Radiographic and Mechanical Study of Epiphyseal Staples," tech. rep., 2001.

[53] M. G. Alonso, A. Yawny, and G. Bertolino, "A tool for solving bone growth related problems using finite elements adaptive meshes," *Journal of the Mechanical Behavior of Biomedical Materials*, vol. 126, 2022.

[54] S. Sadeghian, C. Lewis, and S. Shefelbine, "Can pelvic tilt cause cam morphology? A computational model of proximal femur development mechanobiology," *Journal of Biomechanics*, vol. 157, 2023.

[55] E. M. Manoff, M. B. Banffy, and J. J. Winell, "Relationship between Body Mass Index and slipped capital femoral epiphysis," *Journal of pediatric orthopedics*, vol. 25, pp. 744–746, 11 2005.

[56] D. C. Perry, D. Metcalfe, S. Lane, and S. Turner, "Childhood Obesity and Slipped Capital Femoral Epiphysis," *Pediatrics*, vol. 142, 11 2018.

[57] S. Piszczatowski, "Geometrical aspects of growth plate modelling using Carter's and Stokes's approaches," *Acta of Bioengineering and Biomechanics*, vol. 14, no. 1, 2012.

[58] P. Yadav, S. J. Shefelbine, E. Pontén, and E. M. Gutierrez-Farewik, "Influence of muscle groups' activation on proximal femoral growth tendency," *Biomechanics and Modeling in Mechanobiology*, vol. 16, pp. 1869–1883, 12 2017.

[59] S. Piszczatowski, "Material aspects of growth plate modelling using Carter's and Stokes's approaches," *Acta of Bioengineering and Biomechanics*, vol. Vol. 13, no. no. 3, pp. 3–14, 2011.

[60] C. Hueter, "Anatomische Studien an den Extremitätengelenken Neugeborener und Erwachsener," *Archiv für Pathologische Anatomie und Physiologie und für Klinische Medicin*, vol. 28, pp. 253–281, 5 1863.

[61] R. Volkmann, "Chirurgische Erfahrungen über Knochenverbiegungen und Knochenwachsthum," *Archiv für Pathologische Anatomie und Physiologie und für Klinische Medicin*, vol. 24, pp. 512–540, 9 1862.

[62] A. Arkin and J. Katz, "The effects of pressure on epiphyseal growth; the mechanism of plasticity of growing bone.," *The Journal of bone and joint surgery. American volume*, vol. 38 A, no. 5, 1956.

[63] J. W. Smith, "The relationship of epiphysial plates to stress in some bones of the lower limb," *Journal of Anatomy*, vol. 96, no. Pt 1, p. 58, 1962.

A Patient data - SCFE femur

Variable	**Value**
Gender	Female
Age (years)	11
Affected side	Left
Height (cm)	163
Mass (kg)	77
Head-shaft angle (°)	35
Alpha angle (°)	74
Head-neck offset ratio	0.069
Displacement from Klein's Line (mm)	2

Table A.1: Patient data of the SCFE patient at baseline OK. The left femur is used for the SCFE study.

Note that scans from the same patient are used for both the healthy growth study and the SCFE study. The right femur is used for the former and the left femur is used for the latter.

B Segmentation parameters healthy femur - ABAQUS method

Mimics segmentation	
Threshold bone	196-1404 HU
Average HU value cortical bone	947
Alpha	0.468
Beta	0.000456
Remove spikes	
Spike size	1.0
Smoothing	
Smooth factor	1.0
Number of iterations	3
Reduce parameters	
Geometrical error	0.1
Number of iterations	5
Quality Preserving Reduce Triangles	
Shape quality threshold	0.4
Maximum geometrical error	0.2
Maximum triangle edge length	1.5
Number of iterations	3
Uniform remesh	
Maximum edge length	1.5
Volume mesh	
Element type	Tet4
Maximum edge length	1.5
Shape measure	Aspect ratio (A)
Shape quality threshold	25.0

Table B.1: Segmentation parameters for segmentation of the healthy femur from the CT scan of the healthy growth patient with the ABAQUS method.

C Segmentation parameters healthy femur - MIMICS method

Mimics segmentation	
Threshold bone	196-1404 HU
Average HU value cortical bone	947
Alpha	0.468
Beta	0.000456
Remove spikes	
Spike size	1.0
Smoothing	
Smooth factor	1.0
Number of iterations	3
Reduce parameters	
Geometrical error	0.1
Number of iterations	5
Quality Preserving Reduce Triangles	
Shape quality threshold	0.4
Maximum geometrical error	0.2
Maximum triangle edge length	1.5
Number of iterations	3
Uniform remesh	
Maximum edge length	1.5
Merge	
Fix Wizard	
Volume mesh	
Element type	Tet4
Maximum edge length	1.5
Shape measure	Aspect ratio (A)
Shape quality threshold	25.0

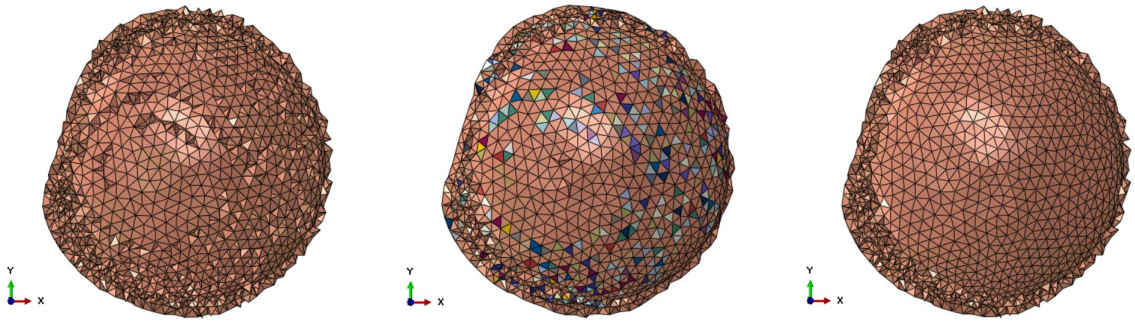
Table C.1: Segmentation parameters for segmentation of the healthy femur from the CT scan of the healthy growth patient with the MIMICS method.

D Segmentation parameters SCFE femur

Mimics segmentation	
Threshold bone	186-2900 HU
Average HU value cortical bone	818.9 HU
HU value estimation in original screw location	333 HU
Alpha	0.500626
Beta	0.000488
Remove spikes	
Spike size	1.0
Smoothing	
Smooth factor	1.0
Number of iterations	3
Reduce parameters	
Geometrical error	0.1
Number of iterations	5
Quality Preserving Reduce Triangles	
Shape quality threshold	0.4
Maximum geometrical error	0.2
Maximum triangle edge length	1.5
Number of iterations	3
Uniform remesh	
Maximum edge length	1.5
Merge	
Fix Wizard	
Volume mesh	
Element type	Tet4
Maximum edge length	1.5
Shape measure	Aspect ratio (A)
Shape quality threshold	25.0

Table D.1: Segmentation parameters for segmentation of the SCFE femur from the the CT scan of the SCFE patient.

E Segmented growth plate material elements



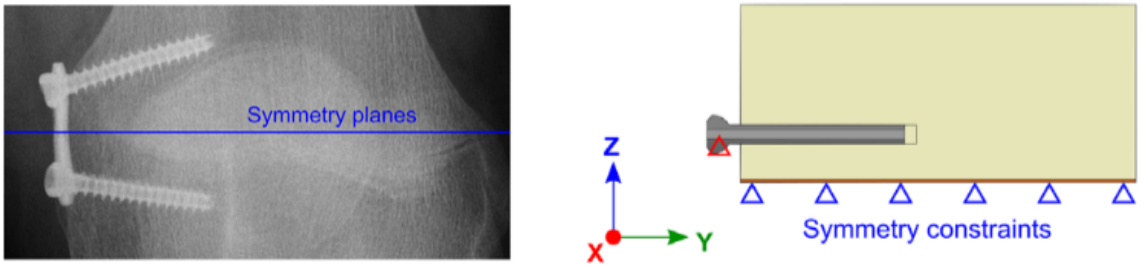
(a) (b) (c)

Figure E.1: a) The elements with growth plate material properties after material assignment by mask in MIMICS b) the smooth growth plate with the elements with the wrong material properties assigned (all non-pink elements) and c) the growth plate material elements after the missing elements have been assigned growth plate material properties in ABAQUS.

F Bone-implant interaction in literature

F.1 The findings of Schneider et al. [51].

The study by Schneider et al. [51] performed FE simulations on a simplified version of the distal femur with an Eight-Plate implant system (Orthofix Inc., Lewisville, TX). A radiograph of this implant system is shown in Figure F.1a and the corresponding FE-model geometry is shown in Figure F.1b. The study simulated bone growth by means of thermal expansion and modelled different combinations of the value for the screw head offset from the bone block ($o_s = 1 - 5$ mm) and the applied temperature change ($\Delta T = 0 - 250$ K) and compared the coordinates of the deformed screw in the FE analysis to the coordinates obtained from radiographs. They selected the combination that best matched clinical data (radiographs after avg. 224 days of growth) as the combination that had the minimal root mean square error of the Y-components of the screw shaft coordinates compared to the radiograph-based coordinates as: $o_s = 2$ mm and $\Delta T = 150$ K for the varus-valgus deformity (VVD) cases. Using these values in the FE analysis, they computed the reaction force of the screw on the growth plate and found that the possible range for the reaction force of the screw on the femur F_g was between $129 - 580$ N for cases of VVD treatment with an Eight-Plate implant.



(a) (b)

Figure F.1: a) Radiograph showing the Eight-Plates and screws in the distal femur and b) the corresponding FE-model geometry (with YZ-plane cut to show screws) and constraints used in the study. Source: [51].

F.2 The findings of Alonso et al. [53]

The results of the growth pressure (i.e. the pressure exerted by growth of the growth plate) appearing around the Blount staple in the distal femur after simulating 50 days and 100 days of growth are shown in Figure F.2. With time, compressive stresses arise between the staple legs, while tensile stresses appear on the diaphyseal zone next to the staple.

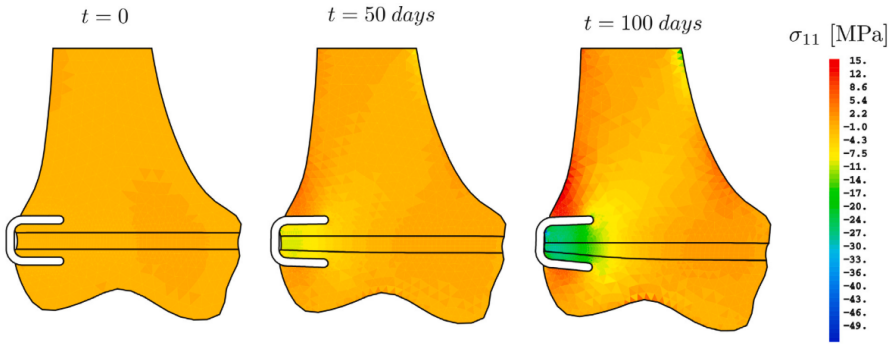


Figure F.2: Stresses in the distal femur arising 50 and 100 days after Blount staple placement. Source: [53].

F.3 The findings of Hucke et al. [50]

Figure F.3 shows the results of the study by Hucke et al. [50] in the form of the stresses in the growth plate at different points in time. It shows that the hydrostatic stresses in the proximity of the implant are reduced right after placing the implant (M2) compared to the stresses before implant placement (M1). At the end of treatment, but with the implant still present, stresses have built in the area of the implant (M3).

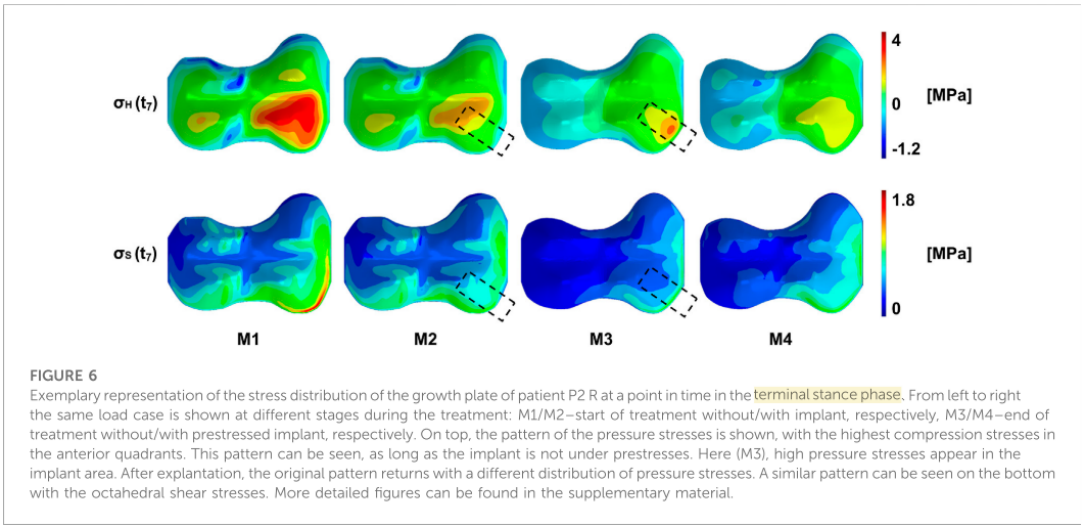


FIGURE 6
Exemplary representation of the stress distribution of the growth plate of patient P2 R at a point in time in the terminal stance phase. From left to right the same load case is shown at different stages during the treatment: M1/M2–start of treatment without/with implant, respectively, M3/M4–end of treatment without/with prestressed implant, respectively. On top, the pattern of the pressure stresses is shown, with the highest compression stresses in the anterior quadrants. This pattern can be seen, as long as the implant is not under prestresses. Here (M3), high pressure stresses appear in the implant area. After explantation, the original pattern returns with a different distribution of pressure stresses. A similar pattern can be seen on the bottom with the octahedral shear stresses. More detailed figures can be found in the supplementary material.

Figure F.3: Stresses in the growth plate right before implant placement (M1), right after implant placement (M2), right before implant removal (M3), right after implant removal (M4). Source: [50].

G Biological growth rate computation

Using the method proposed by [21], the constant biological growth rate can be computed as follows: Previous studies reported that the growth rate in the proximal femur is approximately

$$\text{growth rate} = \frac{d(l)}{dt} = 9 \text{ mm/year} \tag{16}$$

for a seven year old child [44]. This is approximately

$$\frac{d(l)}{dt} = 0.75 \text{ mm/month} \tag{17}$$

The specific growth is then

$$\dot{\epsilon} = \frac{d(l)}{l \cdot dt} = \frac{0.75}{3} = 0.25 \text{ month}^{-1} \tag{18}$$

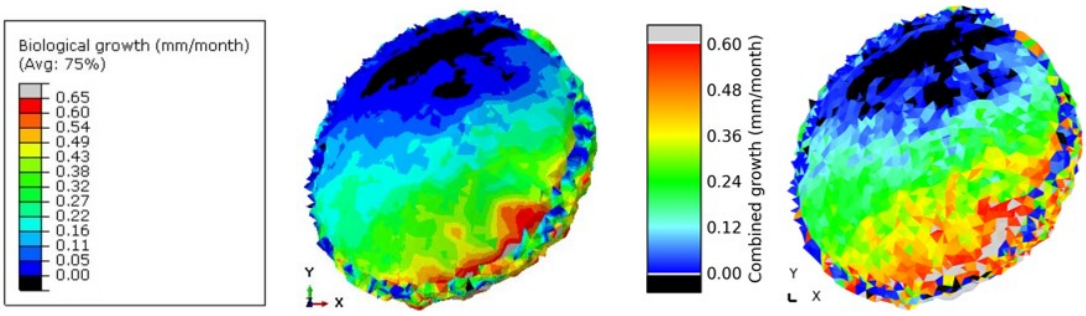
for a growth plate thickness of $l = 3\ mm$. Now using the assumption that the mechanical contribution to bone growth is equal to half of the biological contribution of bone growth [45, 46], growth equation (9) can be rewritten into

$$\dot{\epsilon} = 1.5 \cdot \dot{\epsilon}_b \tag{19}$$

such that

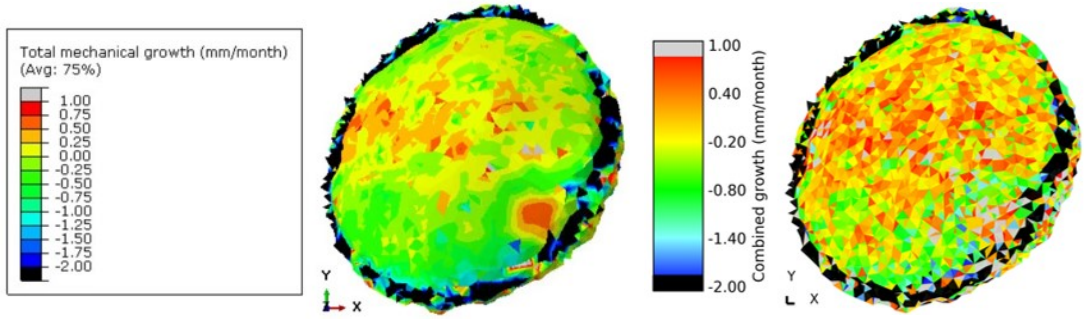
$$\dot{\epsilon}_b = \frac{\dot{\epsilon}}{1.5} = 0.167 \text{ month}^{-1} \tag{20}$$

H ABAQUS versus Python visualisation



(a) (b)

Figure H.1: The biological growth plotted using a) ABAQUS and b) Python (script by author).



(a) (b)

Figure H.2: The total mechanical growth plotted using a) ABAQUS and b) Python (script by author).

I Python scripts

Multiple Python scripts were written for the data processing and analysis in this study. The purpose of each script and the required inputs are briefly summarised below. The scripts may be shared upon request.

- **Write screw to file:** this script writes the element labels of the screw to a file for all screw configurations. This script can be used in ABAQUS directly. The created screw elements file is used in almost all other scripts.
- **Compute average biological growth:** this script computes the average biological growth value for all screw positions over all elements in the growth plate. It requires the *Screw element numbers* files and the *biological growth* files as input.
- **Compute average total mechanical growth:** this script computes the average total mechanical growth value for all screw positions over all elements in the growth plate. It requires the *Screw element numbers* files and the *biological growth* files as input.
- **Bar plot biological and mechanical growth ratio:** this script creates a bar plot showing the biological and mechanical growth rate contribution ratio. It uses the output files of the two previously mentioned scripts as input.
- **Calculate combined growth:** this script calculates the combined growth value in every element in the growth plate using the *biological growth* files and *total mechanical growth* files as input. It writes the combined growth value per element label to a file.
- **Combined growth visualisation:** this script uses the combined growth value per element from the output file created with the previous script and the .inp files of all ABAQUS models (all screw positions) containing the nodal coordinates and element connectivity to create a 3D plot of the combined growth in the growth plate.
- **Sensitivity biological:** This file computes the average strain value in the growth plate, for the sensitivity study of the BIOLOGICAL growth. The thermal expansion coefficient α is decided based on the results of this script.
- **Sensitivity mechanical:** This file computes the average OI value in the growth plate, for the sensitivity study of the MECHANICAL growth. The a and b values (given that b/a=0.5) are decided based on the results of this script.
- **Visualisation biological:** This script is used for the 'ABAQUS versus Python visualisation' section in this report. It creates a visualisation of the biological growth (with the same methodology as used in the script to visualise the combined growth) to be able to compare the visualisation realised with this script to the visualisation by ABAQUS (as used in the study for biological and total mechanical growth).
- **Visualisation mechanical:** This script is used for the 'ABAQUS versus Python visualisation' section in this report. It creates a visualisation of the total mechanical growth (with the same methodology as used in the script to visualise the combined growth) to be able to compare the visualisation realised with this script to the visualisation by ABAQUS (as used in the study for biological and total mechanical growth).